Geological Society of America Bulletin

Stable isotope evidence for topographic growth and basin segmentation: Implications for the evolution of the NE Tibetan Plateau

Brian G. Hough, Carmala N. Garzione, Zhiai Wang, Richard O. Lease, Douglas W. Burbank and Daoyang Yuan

Geological Society of America Bulletin published online 8 October 2010;
doi: 10.1130/B30090.1

Published online October 8, 2010; doi:10.1130/B30090.1

Stable isotope evidence for topographic growth and basin segmentation: Implications for the evolution of the NE Tibetan Plateau

Brian G. Hough[1,*], Carmala N. Garzione[1], Zhicai Wang[2], Richard O. Lease[3], Douglas W. Burbank[3], and Daoyang Yuan[4]
[1]*Department of Earth & Environmental Sciences, University of Rochester, Rochester, New York 14627, USA*
[2]*State Key Laboratory of Earthquake Dynamics, Institute of Geology, China Earthquake Administration, Beijing 100029, China*
[3]*Department of Earth Science, University of California, Santa Barbara, California 93106, USA*
[4]*Lanzhou Institute of Seismology, China Earthquake Administration, Lanzhou 730000, China*

ABSTRACT

Lithologic, magnetostratigraphic, and stable isotope records from the Neogene Xunhua and Linxia basins along the Tibetan Plateau's northeastern margin suggest that topography in the intervening Jishi Shan mountain range began to develop between 16 and 11 Ma. Perturbations to local climate patterns resulting from the evolution of local topography are tracked through comparison of stable isotope compositions of calcareous basin-fill materials across the Jishi Shan. Similarity of isotopic compositions is interpreted to reflect the presence of integrated basins, whereas distinct isotopic compositions reflect unique basin hydrologies. Divergent isotope trends develop between ca. 16 and 11 Ma and are indicative of hydrologic separation in the adjacent Xunhua and Linxia basins and increased aridity in the leeward Xunhua basin. The development of aridity in the lee of the growing topography along the plateau's northeast margin highlights the importance of evaporative enrichment in this extremely continental setting and explains the presence of anomalously positive $\delta^{18}O$ values in modern rainfall. Our findings add to a growing body of evidence for deformation along the plateau's north and northeastern margins in the middle to late Miocene.

INTRODUCTION

Cenozoic uplift of the Tibetan Plateau is generally regarded as a primary driving factor in seasonal shifts in the amount of precipitation received by coastal Asia (Ruddiman and Kutzbach, 1989; Raymo and Ruddiman, 1992; Araguás-Araguás et al., 1998). In addition to increased seasonality of rainfall, uplift of the Tibetan Plateau has also led to the Miocene aridification of the northern Tibetan Plateau (Guo et al., 2002; Dettman et al., 2003; Graham et al., 2005; Kent-Corson et al., 2009). Aridification of the northern Tibetan Plateau can be ascribed to orographic blocking of vapor transport pathways. It has been suggested that the resulting climate change should scale with the amount and extent of surface uplift and coincide with the timing of plateau uplift (Kutzbach et al., 1989; Ruddiman and Kutzbach, 1989; Molnar et al., 1993; Hsu and Liu, 2003). Characterization of the changes in paleoclimate, as well as their patterns in space and time, should mimic patterns of deformation associated with growth of the Tibetan Plateau.

The timing and nature of topographic growth along the NE margin of the Tibetan Plateau are recorded in part by the age, distribution, and duration of sedimentary deposits along the plateau margin (Fang et al., 2003, 2005; Zheng et al., 2003; Horton et al., 2004; Dupont-Nivet et al., 2004; Lease et al., 2007). Numerous small basins exist along the plateau margin, but they are currently separated by high-standing ranges and/or basement highs (Fig. 1). The stratigraphy within these basins shows similar lithologies and ages, suggesting that these basins may have formed as parts of a larger basin (e.g., the Xining-Minhe basin; Zhai and Cai, 1984; Horton et al., 2004) early in their history that was later segmented by the relatively recent growth of intervening ranges. Alternatively, these basins may have developed individually within a preexisting landscape such that local deformation is relatively old. If the Tibetan Plateau grew progressively outward through time, evidence from basins situated along the NE margin of the plateau should reveal a single depositional history, interrupted by recent basin segmentation and tectonic activity. Therefore, documenting the age, style, and order of basin segmentation along the margin of the Tibetan Plateau is an important first step toward an understanding of the overall pattern of deformation associated with plateau growth.

Climatic change associated with the development of orographic barriers may be recorded in sedimentary basin deposits, thereby providing a history of the growth of intervening ranges (e.g., Kleinert and Strecker, 2001). Sedimentary rock can record changes in local climate through the stable isotopes of sedimentary carbonate, which reflects the isotopic composition of meteoric water (Cerling and Quade, 1993). Orographic effects resulting from the emergence of a mountain range may lead to the development of a rain shadow, where rainfall amounts increase on the windward side of the range and decrease on the leeward side. As water vapor is forced to ascend to higher altitudes, it cools, condenses, and rains out, thereby increasing the fractionation of oxygen isotopes and lowering the $\delta^{18}O$ values of the vapor mass and precipitation (Dansgaard, 1964; Rozanski et al., 1993). On the leeward side of several coastal mountain ranges, depleted $\delta^{18}O$ values have been observed associated with the "rain shadow effect" (e.g., Chamberlain et al., 1999; Poage and Chamberlain, 2001; Takeuchi and Larson, 2005). However, regions with extreme continentality, such as NE Tibet, show a different pattern of isotopic composition of precipitation. On the drier, leeward side of the mountains, a less well-recognized process of evaporative enrichment of raindrops can cause the $\delta^{18}O$ values of precipitation ($\delta^{18}O_{rw}$) to increase (Lee et al., 2007; Lee and Fung, 2008). This "evaporative enrichment" in ^{18}O counterbalances and may even outweigh the decrease in $\delta^{18}O_{rw}$ associated with the altitude effect on the windward side of the range.

Along the northeast margin of the Tibetan Plateau, the Linxia and Xunhua basins represent

*E-mail: bhough@earth.rochester.edu

GSA Bulletin; doi: 10.1130/B30090.1; 7 figures; 2 tables; Data Repository item 2011008.

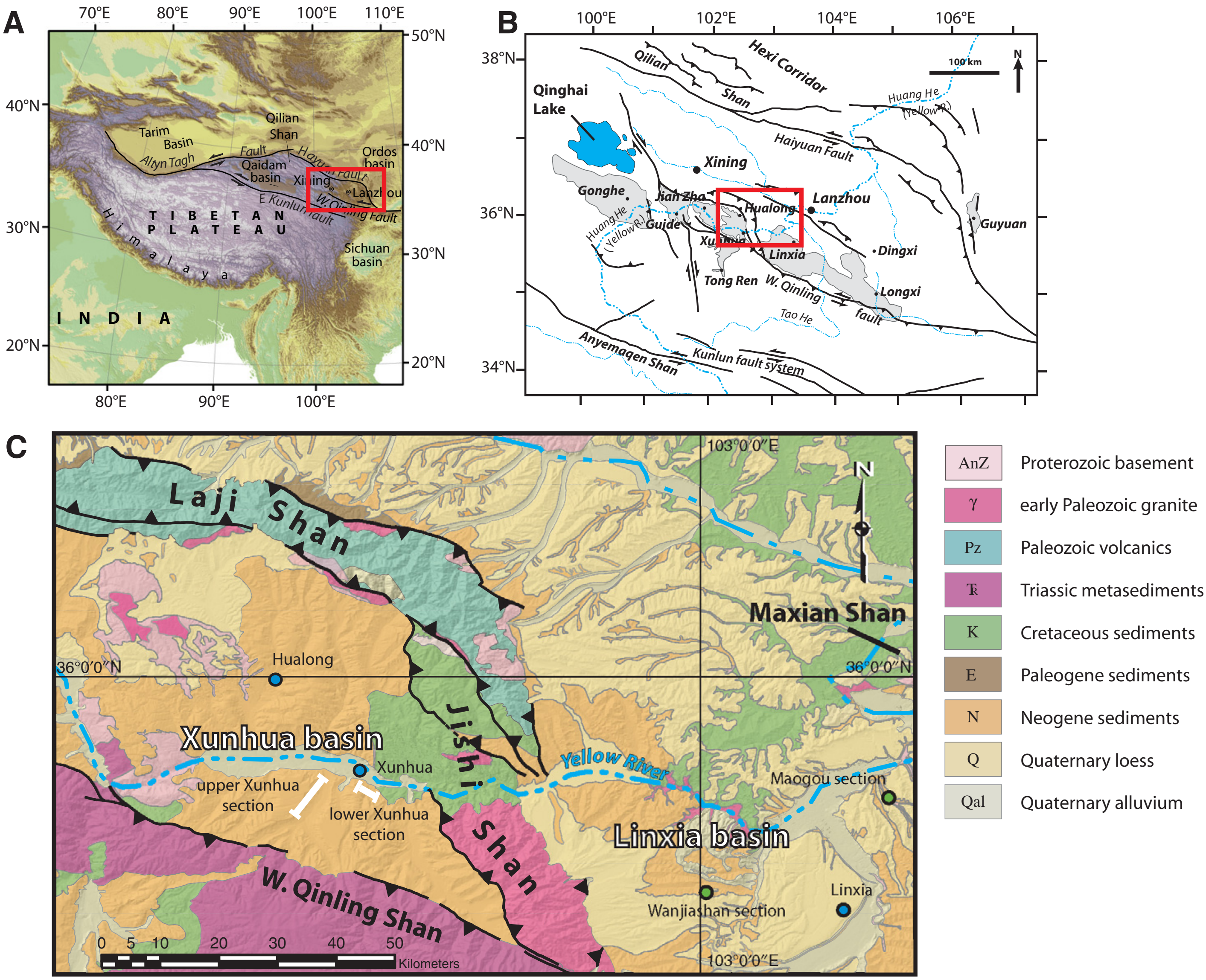

Figure 1. (A) Regional shaded relief map of Tibet showing major physiographic and tectonic features of the Tibetan Plateau. Red box outlines extent of B. (B) Generalized tectonic map of the northeast margin of the Tibetan Plateau (modified from Horton et al., 2004). Gray shading indicates extent of Neogene sedimentary basins. Heavy black lines indicate major faults. Dashed blue lines indicate modern river systems that drain the region. Red box outlines study area and extent of C. (C) Geologic map of the study area showing locations of measured sections and extent of Neogene fill. γ—early Paleozoic granite, AnZ—Proterozoic metamorphic basement, Tr—Triassic metasediments, Pz—Paleozoic volcanics, K—Cretaceous clastic sediments, E—Paleogene fluviolacustrine sediments, N—Neogene fluvial and lacustrine sediments, Q—Quaternary loess, Qal—Quaternary alluvium (modified from Gansu Bureau of Geology and Mineral Resources, 1989; Qinghai Bureau of Geology and Mineral Resources, 1991).

an example of two such basins occupying windward and leeward positions with respect to the intervening Jishi Shan mountain range. The Jishi Shan, a 3500-m-high, 35-km-wide mountain range, currently separates the Xunhua basin from the Linxia basin. The Linxia basin (Figs. 1B and 1C) contains up to 1200 m of sedimentary rock that constitutes a nearly continuous record of sediment accumulation from 29 to 1.8 Ma (Fang et al., 2003). The Xunhua basin (Figs. 1B and 1C) contains more than ~1500 m of sedimentary fill, and based on proximity, section thickness, and mapped lithologies (Qinghai Bureau of Geology and Mineral Resources, 1991), it appears to span a time range similar to that reported for Linxia basin deposits.

The goal of this study is to determine the timing of the development of topography along the NE margin of Tibet in order to establish when high-standing ranges, such as the Jishi Shan, began to emerge. Here, we place temporal constraints on the Xunhua sedimentary record through comparison of new detailed lithostratigraphic, chemostratigraphic, and magnetostratigraphic records from the Xunhua basin with established records in the Linxia basin (Fang et al., 2003; Dettman et al., 2003; Garzione et al., 2005). Our approach is to examine modern rainfall to characterize stable isotope compositions ($\delta^{18}O$ and δD) within the modern climatic setting of the Linxia and Xunhua basins. Through comparison of $\delta^{18}O$ values in modern soil carbonates to those in rainfall, we evaluate the extent of evaporative enrichment between meteoric water and soil carbonates. Finally, by comparing modern trends in the isotopic composition of rainfall ($\delta^{18}O_{rw}$ and δD_{rw}) and soil carbonate ($\delta^{18}O_{sc}$ and $\delta^{13}C_{sc}$) to pedogenic and lacustrine carbonate records ($\delta^{18}O_c$ and $\delta^{13}C_c$) from Linxia and Xunhua basins, we interpret paleohydrology and paleoclimate trends between the basins to evaluate when the Jishi Shan became an important topographic feature. Through this study, we explore the processes that lead to heavy isotope (^{18}O and D) enrichment in continental interior regions, which is counter to the expected trend toward more negative $\delta^{18}O_{rw}$ and δD_{rw} values associated with distillation of vapor masses. In addition, we compare the stable isotopic record of climate change and topographic growth in NE Tibet to studies further to the west to evaluate the regional patterns of aridification associated with topographic growth of the Tibetan Plateau.

GEOLOGIC SETTING

Plateau Margin

As the Tibetan Plateau has grown outward toward the northeast (e.g., Bally et al., 1986; Molnar et al., 1993; Métivier et al., 1998; Meyer et al., 1998; Tapponnier et al., 2001; E. Wang et al., 2006), it has disrupted the previously continuous, low-lying topography and altered local- to regional-scale climate patterns. Cretaceous sedimentation in the foreland of the Kunlun Shan generated a succession of red clastic strata dominantly composed of sandstone and poorly sorted, subangular to subrounded, pebble-to-cobble conglomerates that are well indurated and locally contain abundant burrows. These regionally extensive deposits occupy the Jurassic–Cretaceous Xining-Minhe basin (Horton et al., 2004) and underlie several smaller Neogene basins to the south and west (e.g., Guide, Xunhua, Hualong, Jian Zha, and Tong Ren basins) (Fig. 1C). These Cretaceous deposits are also preserved on top of some intervening mountain ranges, such as the Maxian Shan, Laji Shan, Jishi Shan, and W. Qinling Shan (Fig. 1B) (Qinghai Bureau of Geology and Mineral Resources, 1991; Gansu Bureau of Geology and Mineral Resources, 1989), indicating that subsequent tectonic processes were responsible for the deformation of these high-standing ranges.

Our study area, located near the border between Qinghai and Gansu provinces on the northeastern margin of the Tibetan Plateau, includes the Xunhua and Linxia basins (Figs. 1B and 1C). These basins are situated at ~1800–2000 m above sea level and contain thick successions of Neogene deposits (Qinghai Bureau of Geology and mineral Resources, 1991; Gansu Bureau of Geology and Mineral Resources, 1989). During the Miocene, the Linxia basin was intermittently a closed drainage basin (Dettman et al., 2003; Fang et al., 2003), and, based on similarity of sedimentation between the Linxia and adjacent Xunhua basins (described herein), the Xunhua basin is likely to have aggraded synchronously with Linxia.

The prominent east-west–trending Laji Shan and north-south–trending Jishi Shan are narrow (20–30 km), 3500-m-high ranges (4280 m maximum height; 3000 m mean crest height) that separate the Linxia basin from the Xunhua basin (Fig. 1B). Exhumation of rock in the Laji Shan–Jishi Shan at ca. 8 Ma has been interpreted from magnetostratigraphic, detrital zircon U/Pb ages, and detrital apatite fission-track data from the Linxia basin and the nearby Guide basin (Fang et al., 2003, 2005; Zheng et al., 2003; Lease et al., 2007)(Fig. 1B). The Linxia basin contains dated sedimentary rocks spanning 29–1.8 Ma (Fang et al., 2003), and therefore should record the development of basin-segmenting topography as well as any associated orographically induced localized climate change.

Xunhua Basin Stratigraphy

The Xunhua basin (elevation ~1900 m at the Yellow River) contains >1500 m of Neogene sediments that lie unconformably over Cretaceous sandstones and conglomerates in the east and on Proterozoic granodiorites in the west. The southern edge of the basin is bounded by the West Qinling range, and the northern edge is bounded by the Laji Shan (Fig. 1C).

We measured 1500 m of Neogene sedimentary rocks within two sections in the south-central part of the Xunhua basin (Figs. 1C and 2). As detailed in the following, Neogene sediments within the lower Xunhua section generally fine upward from sandy deltaic–floodplain facies to silt- and clay-rich lacustrine facies. We estimate a gap of 700–800 m between the lower and upper Xunhua sections based on a nearly constant bedding orientation (55° to 290°) from the top of the lower section to a distinct green marker bed that crops out above the lower Xunhua measured section and marks the base of the upper Xunhua section. Sedimentary rock in the upper Xunhua section was deposited in four distinct environments (lacustrine, marginal lacustrine, fluvial/floodplain, and braided fluvial) that exhibit an overall coarsening-upward trend.

Lower Xunhua Section

We measured 530 m of sedimentary rock within the lower Xunhua section (Fig. 2) where the beds dip an average of 54° toward 286°. The base of our section lies near the lowest-elevation deposits exposed in a continuous section by the Yellow River. Older deposits lie beneath these, but they have yet to be exhumed by the Yellow River. The lower Xunhua section is composed of two distinct units. The basal unit of the lower section contains two subunits. The first subunit exists from 0 to 70 m and consists of dark red, lenticular, very thickly bedded, poorly sorted, massive, silty coarse-grained sandstones that extend laterally for hundreds of meters. These sandstones contain rare tan to greenish-white, lenticular interbeds of thickly bedded, massive, matrix-supported, pebble-to-cobble conglomerate with clasts composed of subrounded Triassic metasedimentary rock. Conglomerate interbeds are laterally continuous over 10–100 m. The second subunit (from 70 to 265 m) contains red-brown, lenticular, thinly to thickly bedded, massive to horizontally laminated, silty sandstones that are laterally extensive over hundreds of meters and contain rare gypsum veins (<1 cm thick) oriented at an angle to bedding. We interpret the sandy grain sizes, the lenticular bedding, and the limited lateral continuity of the beds in the basal unit to represent a fluvial environment. The contact between the fluvial deposits below 265 m and the overlying deposits is gradational over ~10–15 m. The second unit grades to a dark red to brown, silt- and clay-rich, tabular, medium- to thick-bedded, massive, silt to very fine sandstone that is laterally continuous over hundreds of meters and persists through the top of the section. Two distinct subunits are found within this sandstone unit. The first subunit exists between 340 and 365 m, and it consists of calcareous, massive mudstone that is laterally continuous over tens to hundreds of meters and contains abundant root traces, and discrete calcareous horizons. These attributes suggest that this subunit represents multiple floodplain paleosols. The second subunit exists from 410 to 465 m and is composed of dark red-brown, tabular, massive, siltstone with tan and bluish-green mottling and rare vein gypsum that both parallels and crosscuts bedding. From 465 m through the top of the section, vein gypsum becomes thicker (5–10 cm) and more abundant. Near the top of the section, several distinctive blue-green, ledge-forming beds up to 1 m thick contain gypsum-rich flower and vein morphologies. Based on the fine grain size, tabular bedding, and extensive evaporite deposition at the top of the section, we interpret this part of the lower Xunhua section to represent a lacustrine depositional environment.

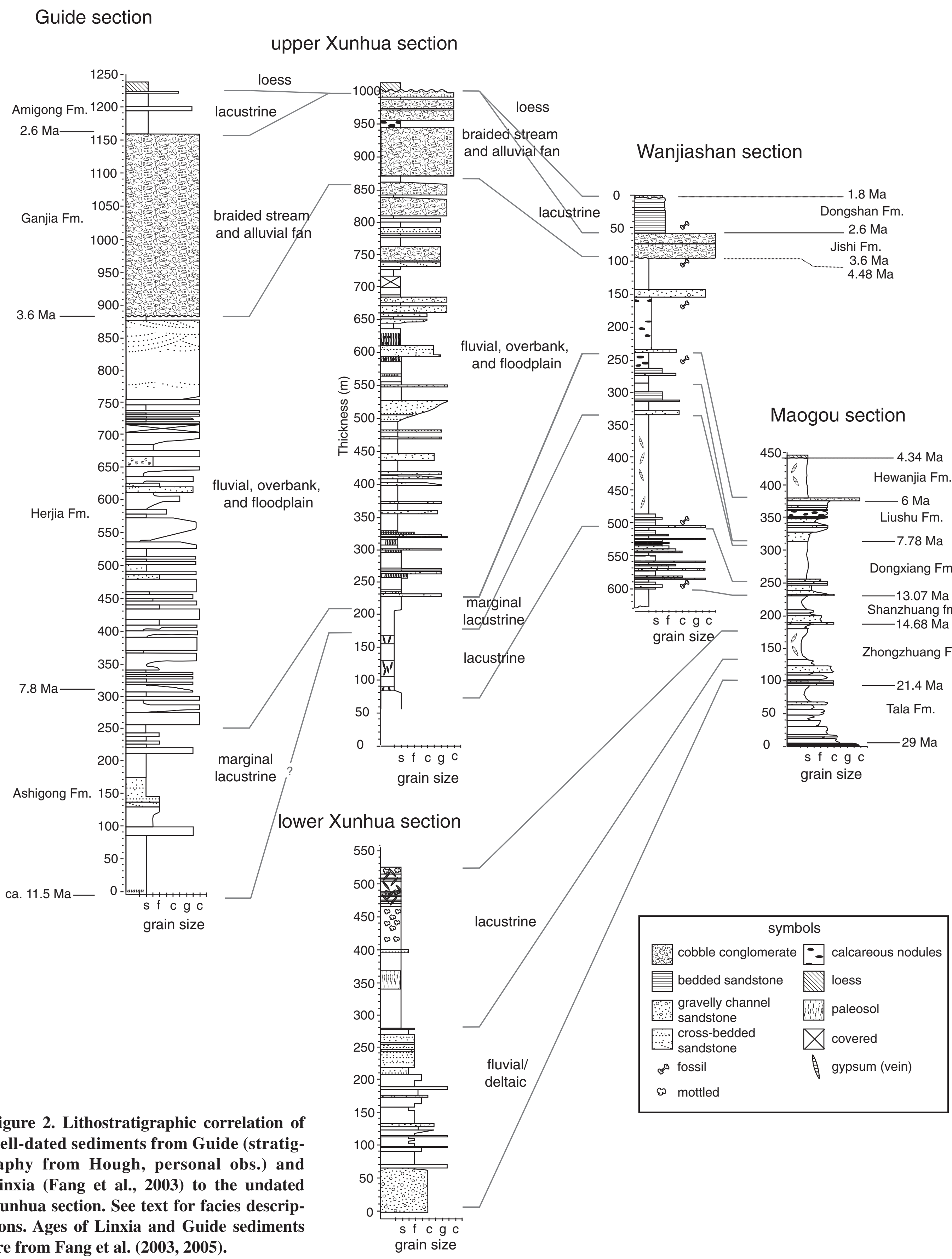

Figure 2. Lithostratigraphic correlation of well-dated sediments from Guide (stratigraphy from Hough, personal obs.) and Linxia (Fang et al., 2003) to the undated Xunhua section. See text for facies descriptions. Ages of Linxia and Guide sediments are from Fang et al. (2003, 2005).

Upper Xunhua Section

We measured 995 m of sedimentary rock in the upper Xunhua section (Fig. 2) where the beds dip at an average of 6° toward 221°. The bottom ~175 m contains calcareous mudstone with abundant interbedded gypsum, gypsum veins that crosscut bedding, and gypsum flowers. Individual beds can be traced over several kilometers of outcrop. These deposits (locally described as "zebra striped") exhibit an alternating pattern of reddish-brown/purple mudstone and white/green calcareous and/or gypsiferous mudstone (Fig. 3E). We interpret these as lacustrine deposits that are lithologically correlative to the 13.07–7.56 Ma lacustrine Dongxiang Formation in the Linxia basin (Fang et al., 2003). The zebra-striped deposits are overlain by yellow/brown laminated, lacustrine mudstone interbedded with massive, mottled, and bioturbated mudstone and medium-bedded, fine- to coarse-grained

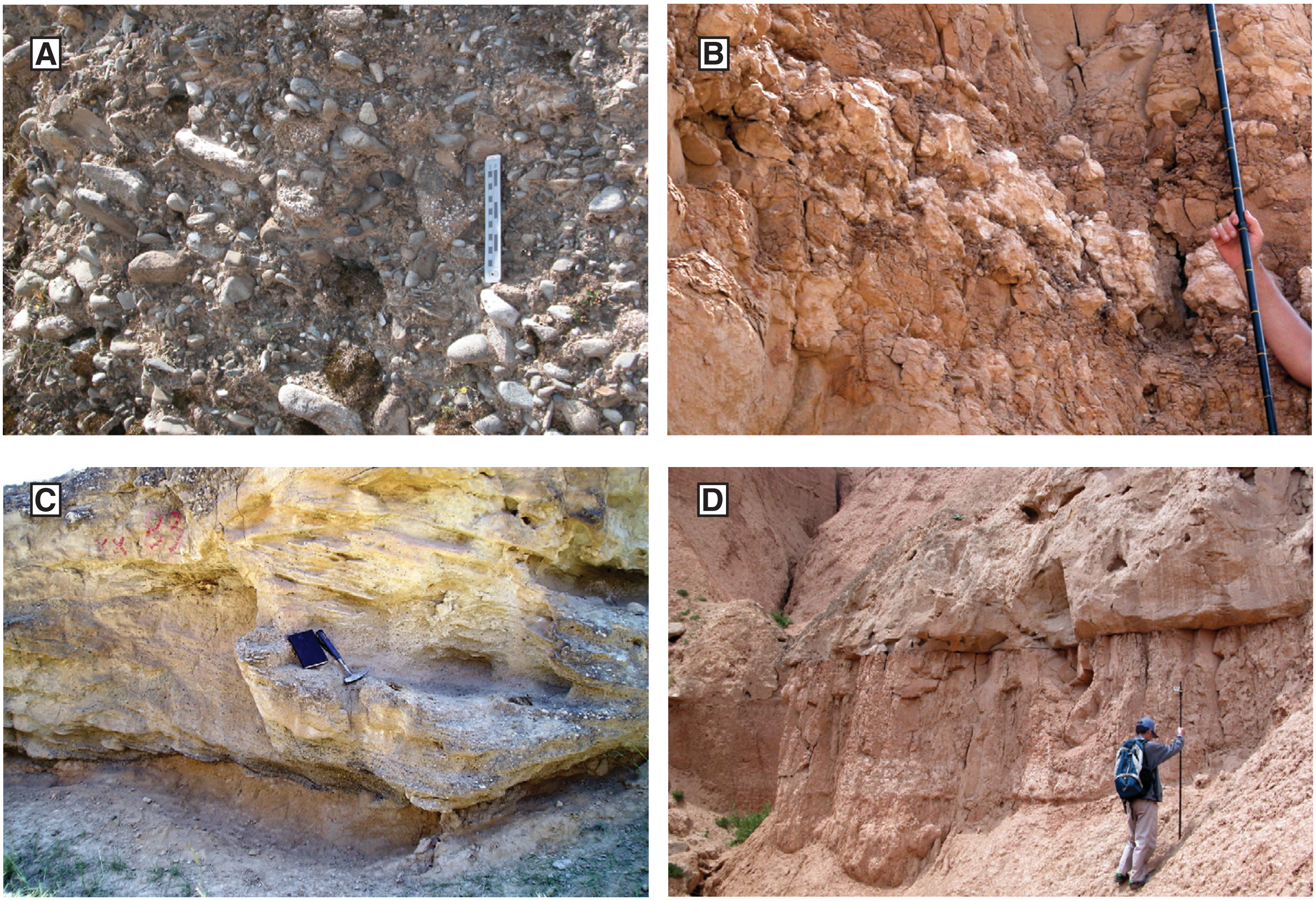

Figure 3. Photographs of lithologies found in the Xunhua section: (A) Jishi Formation equivalent imbricated cobble conglomerate found from 865 to 995 m in upper Xunhua section; (B) soil carbonate layers common in the interval between 570 m and 630 m in the upper Xunhua section; (C) cross-stratified channel sandstone common above 750 m in the upper section; (D) stacked paleosols capped by channel sandstone found at ~620 m in the upper section, and (E) dark red lacustrine micrites with green calcareous/gypsiferous interbeds common above 280 m in the lower section and from 0 to 210 m in the upper section. Grain size abbreviations: s—silt; f—fine sand; c—coarse sand; g—granule, c—cobble.

massive sandstone in the stratigraphic interval between 175 and 225 m. We interpret these deposits as marginal lacustrine facies correlative to that of the 7.56–6 Ma Liushu Formation in the Linxia basin (Fang et al., 2003).

These marginal lacustrine deposits coarsen upward, giving way to interbedded red-brown, massive sandstones and light brown, massive, calcareous mudstones between 225 and 865 m (Fig. 3D). We interpret this interval as fluvial channel and floodplain deposits that include numerous stacked paleosols (Mack et al., 1993). Paleosols typically lack a well-defined A horizon, but they are identified by abundant root traces, blocky structure, increasing carbonate content with depth, and the presence of carbonate nodules to massive carbonate layers within the lower part of their B horizons (Bk horizons). Typical preserved thicknesses of individual paleosols are between 20 cm and 100 cm (Fig. 3B). Fluvial channel deposits are characterized by trough cross-bedded, medium to coarse lenticular sandstone (Fig. 3C) and by conglomerate with imbricated pebbles and cobbles that are laterally continuous over hundreds of meters. Channel deposits increase toward the top of this part of the section. The interval of fluvial channel and floodplain deposits is lithologically similar to the 6–4.6 Ma Hewanjia Formation in the Linxia basin (Fang et al., 2003).

Between 865 and 995 m, channel deposits of the fluvial facies coarsen upward into thickly bedded, tabular-to-lenticular, massive-to-imbricated sandstone and cobble conglomerate (Fig. 3A). Individual beds extend laterally for tens of meters and stack to form multistory lenticular bodies that extend laterally up to several kilometers. We interpret this interval to represent braided stream deposits within alluvial-fan environments, similar in lithology to the 3.6–2.6 Ma Jishi Formation in the Linxia basin (Fang et al., 2003). A blanket of Quaternary loess caps the section.

The proximity of the Xunhua and Linxia basins, the similarity between lithologies and depositional environments in both basins, and the longevity of continuous sedimentation in the Linxia basin (1.7–29 Ma; Fang et al., 2003) suggest that these basins can be used to track the topographic development of this portion of NE Tibet. Furthermore, the presence of Cretaceous deposits similar to those within the intervening Jishi Shan (Gansu Bureau of Geology and Mineral Resources, 1989) suggests that, prior to emergence of the Laji Shan and Jishi Shan, these basins were depositionally and hydrologically linked. The mere similarity in stratigraphy between these basins does not necessitate synchronous deposition because lithologic boundaries may be time transgressive.

METHODS

Rain collector assemblies and temperature–relative humidity (RH) data loggers were placed in the Linxia and Xunhua basins in May 2007. Mean monthly samples of modern rainfall and hourly measurements of temperature and RH were collected over the course of the 2007 and 2008 summer monsoons.

We constructed rain collector assemblies similar to those of Scholl et al. (1996) (see GSA Data Repository Fig. DR1[1]). Time-integrated precipitation samples for isotopic analysis ($\delta^{18}O_{rw}$ and δD_{rw}) were collected once a month, along with measurements of total monthly rainfall, hourly temperature (°C), and relative humidity (%) from May 2007 through October 2008. To compare to longer-term regional averages, we used monthly average isotopic compositions of rainfall obtained from the International Atomic Energy Agency (IAEA)/Global Network of Isotopes in Precipitation (GNIP) database from nearby Lanzhou (Fig. 1B; Table 1), which was sampled for six years between 1986 and 1997 (IAEA/WMO, 2006).

We analyzed samples of modern rainwater collected between May and September 2007 for δD_{rw} at the University of Georgia's Savannah River Ecology Laboratory. The analyses for δD_{rw} were performed on a TC/EA peripheral device (Thermo Fisher) connected to a Thermo Delta^{PLUS} XL continuous-flow–isotope ratio mass spectrometer (CF-IRMS). Three sample peaks were averaged for each analysis, resulting in 1σ standard deviation of <±1‰. Reference standards included Vienna standard mean ocean water (VSMOW), Greenland Ice Sheet Precipitation (GNIP), and deionized tap water (DITAP). The analytical precision was approximately ±1‰ (1σ).

Rainwater samples collected between October 2007 and October 2008 were analyzed for δD at the University of Arizona and for $\delta^{18}O_{rw}$ at the University of Rochester. δD analyses were performed using a Los Gatos Liquid Water Isotope Analyzer. Sample size was 0.7 L, and samples were injected into a heated line supplying water vapor to the laser chamber. Standardization was based on two internal water standards calibrated to VSMOW and Vienna Standard Light Antarctic Precipitation (VSLAP). Analytical precision based on the repeated analysis of internal standards is ±0.6‰ (1σ). The $\delta^{18}O_{rw}$ analyses were performed on a Thermo Delta^{PLUS} XL CF-IRMS using the GasBench II peripheral device. Six to ten sample peaks were averaged for each analysis, yielding a 1σ standard deviation of <±0.08‰. Two in-house standards, each calibrated to VSMOW, were run after every seventh sample, resulting in an analytical precision of ±0.1‰ (1σ). Isotopic results for both hydrogen and oxygen are reported using standard delta (δ) notation with respect to VSMOW.

Pedogenic carbonate samples were collected from as deep as possible in each soil profile (30–50 cm) to minimize the potential effects of diffusion and evaporation (Cerling and Quade, 1993). We examined each sample under a stereoscopic microscope to identify representative material for subsampling and to segregate potential diagenetic phases from the subsamples. Carbonates were analyzed at the University of Rochester on a Thermo Delta^{PLUS} XL CF-IRMS using the GasBench II peripheral device. Powdered samples were reacted with 30% H_2O_2 for 20 min to remove organic material prior to analysis. Isotopic results for both carbon and oxygen are reported using standard delta (δ) notation with respect to VPDB (Vienna Peedee belemnite). Isotope ratios were calculated using three in-house standards, each calibrated to NBS-19 and NBS-18. Analytical error is ±0.1‰ for $\delta^{18}O_c$ values (1σ) and ±0.06‰ for $\delta^{13}C_c$ (1σ).

Postdepositional alteration (diagenesis) of a carbonate sample may cause resetting of isotope ratios to the time and conditions at which diagenesis occurred (e.g., Garzione et al., 2004). Assessment of the degree and relative timing of diagenetic alteration is, therefore, crucial prior to interpretation of paleoclimate. In the field, samples were collected by avoiding weathered surfaces and visible calcite or gypsum veins. To assess the degree to which diagenetic processes have altered samples, we used a stereoscopic microscope to identify potential diagenetic phases (sparite) in hand sample prior to sample preparation. Diagenetic phases were sampled for comparison of their isotopic composition to unaltered micrite in the same sample to determine the nature of diagenesis.

Thin sections were made of both randomly selected samples throughout the section and

[1]GSA Data Repository item 2011008, Figure DR1: Schematic diagram of the rain collector assembly; Figure DR2: Graph of monthly average of precipitation (mm/day) and a wind rose for the rainiest month (August); Figure DR3: Cross plots of $\delta^{18}O$ and $\delta^{13}C$ showing the degree of covariance in lacustrine sediments from the Xunhua and Linxia basins; Figure DR4: Examples of paleomagnetic results from the upper Xunhua section; Figure DR5: Plot of Relative Isothermal Remanent Magnetism (IRM) moment within an increasing magnetic field from the upper Xunhua section; Figure DR6: Fold test plot; Figure DR7: Magnetostratigaphic jackknife resampling plot; Figure DR8: Sediment accumulation rate graphs; Figure DR9: Alternative correlations for the Xunhua magnetostratigraphy to the GPTS; Table DR1: Rainwater isotope data, is available at http://www.geosociety.org/pubs/ft2011.htm or by request to editing@geosociety.org.

TABLE 1. AVERAGE MONTHLY PRECIPITATION DATA FROM GLOBAL NETWORK OF ISOTOPES IN PRECIPITATION STATION IN LANZHOU, AND FROM RAIN GAUGES IN LINXIA AND XUNHUA

Month	Average			Average			Weighted average		
	Temperature (°C)	Precipitation (mm)	%RH	$\delta^{18}O$	δD	d-excess	$\delta^{18}O$	δD	d-excess
Xunhua (35°51′0″N, 102°28′48″E, 1829 m)									
Jan	–4.4	2.5	48	–12.6	–115.7	–14.9	—	—	—
Feb	–1.6	0.6	43	—	—	—	—	—	—
Mar	7.0	8.8	44	—	—	—	—	—	—
Apr	12.4	13.4	46	–6.5	–37.5	14.5	—	—	—
May	16.9	26.7	48	–0.5	5.8	9.4	–0.3	7.7	10.0
Jun	19.1	51.2	60	–5.3	–28.9	13.5	–5.1	–27.6	13.6
Jul	21.3	95.2	63	–6.9	–42.7	12.5	–6.9	–42.9	12.6
Aug	20.2	68.2	66	–9.5	–59.0	17.0	–9.8	–61.4	17.4
Sep	16.1	57.5	73	–11.0	–74.2	13.8	–10.5	–70.4	13.3
Oct	15.0	13.2	69	–8.9	–59.6	11.6	—	—	—
Nov	2.2	1.3	55	—	—	—	—	—	—
Dec	–3.4	0.2	51	—	—	—	—	—	—
Linxia (35°38′24″N, 103°15′36″E, 1788 m)									
Jan	–7.1	8.3	66	–15.3	–115.3	7.1	—	—	—
Feb	–3.1	2.4	62	–10.0	–62.9	17.1	—	—	—
Mar	4.6	26.0	63	–6.1	–37.9	10.9	—	—	—
Apr	9.2	50.5	60	–1.4	–12.1	–0.9	—	—	—
May	15.3	55.9	58	–2.7	–10.5	11.1	–2.7	–9.9	11.1
Jun	16.8	101.3	70	–4.9	–26.2	12.6	–4.4	–22.7	12.2
Jul	18.6	83.0	73	–7.4	–49.1	9.7	–7.7	–48.2	9.8
Aug	17.8	152.8	78	–10.9	–71.4	15.8	–11.0	–70.1	16.0
Sep	13.2	101.3	81	–11.9	–77.0	18.2	–12.5	–77.5	18.1
Oct	7.7	75.3	82	–10.3	–60.8	21.6	—	—	—
Nov	1.7	6.5	72	—	—	—	—	—	—
Dec	—	—	—	–11.6	–70.3	22.5	—	—	—
Lanzhou GNIP (36°3′00″N, 103°52′48″E, 1517 m)									
Jan	–4.3	0.5	48	–23.7	–157.2	32.4	—	—	—
Feb	0.5	0.5	41	—	—	—	—	—	—
Mar	5.9	8.8	45	–11.8	–87.1	7.2	–11.6	–93.0	–0.4
Apr	12.9	16.2	42	–7.5	–53.5	6.8	–7.9	–57.4	5.8
May	17.5	46.2	47	–5.5	–37.9	5.8	–5.6	–38.3	6.3
Jun	20.7	62.3	53	–4.5	–26.5	9.1	–4.4	–23.6	11.5
Jul	22.4	75.0	58	–3.3	–27.1	3.9	–3.5	–31.6	1.2
Aug	21.7	50.0	58	–7.4	–52.3	7.2	–7.5	–53.7	6.7
Sep	17.1	40.2	57	–4.9	–29.3	10	–6.8	–40.0	14.8
Oct	10.5	21.2	60	–6.9	–50.7	16.6	–7.1	–57.9	20.8
Nov	2.9	0.7	56	–13.1	–87.1	17.5	–14.9	–99.0	20.2
Dec	–3.2	0.7	54	–7.7	–57.4	4.4	—	—	—

Note: GNIP data span the years 1985, 1986, 1996, 1997, 1998, 1999. Data from Linxia and Xunhua span 2007–2008. "—" = no data, which typically results from the lack of rainfall during the respective month. Weighted averages are weighted by precipitation amount and require at least 2 yr of data. RH—relative humidity.

samples with sparite visible under low magnification to more accurately determine the mineral phases (calcite or gypsum) and nature of diagenetic alteration. Petrographic analysis of these samples focused on the identification of the percent sparry calcite and determination of its genesis. Relative timing of diagenetic alteration was determined visually by examining samples for evidence of carbonate dissolution, replacement, recrystallization, or carbonate cementation.

We collected samples for magnetic polarity stratigraphy in mudstones, siltstones, and sandstones from both the lower Xunhua and upper Xunhua sections described earlier in this paper. In the lower section, we collected oriented block samples from 105 sites over 530 m for a sampling density of 5 m/site. In the upper section, we drilled 635 oriented cores from 204 sites over 980 m for a sampling density of ~5 m/site. We drilled all specimens to 2.5-cm-diameter cores and measured their remanent magnetizations using a 2G Enterprises DC SQuID three-axis cryogenic magnetometer housed in a magnetically shielded room at the California Institute of Technology and at Occidental College, which have identical magnetometer and sample-changer instrumentation. The magnetometer has a background noise of <1 pAm^2 and is equipped with computer-controlled alternating field (AF) demagnetization coils and an automated vacuum pick-and-put sample changer (Kirschvink et al., 2008). We performed thermal demagnetization in a magnetically shielded ASCTM oven in either a nitrogen or an oxygen atmosphere.

We initially measured each of 486 specimens for natural remanent magnetization (NRM) with a subset of samples cooled in a liquid nitrogen bath to remove potential multidomain viscous magnetizations. Specimens were then subjected to alternating field (AF) demagnetization in 25 gauss (G) steps up to 100 G to remove low-coercivity magnetizations, and stepwise thermal demagnetization in 8–16 steps between 150 and 680 °C (or 600 °C), typically in (1) 50–100 °C steps up to 450 °C, and (2) 10–50 °C steps up to 680 °C.

MODERN RAINFALL AND MODERN SOIL CARBONATE RESULTS

We examined modern meteoric water (rainfall) to characterize the ground-level variation in the stable isotopes ($\delta^{18}O_{rw}$ and δD_{rw}) within the modern climate regime. Through comparison of $\delta^{18}O$ values in Quaternary soil carbonates to those in rainfall, we evaluated the extent of evaporative enrichment between meteoric water and soil water, and hence soil carbonate.

The modern orographic presence of the Jishi Shan results in a measurable difference in amount of rainfall received at ground level on either side of the range. In 2007–2008, the Linxia basin received 70.1/61.8 cm/yr of rainfall, whereas the Xunhua basin only received

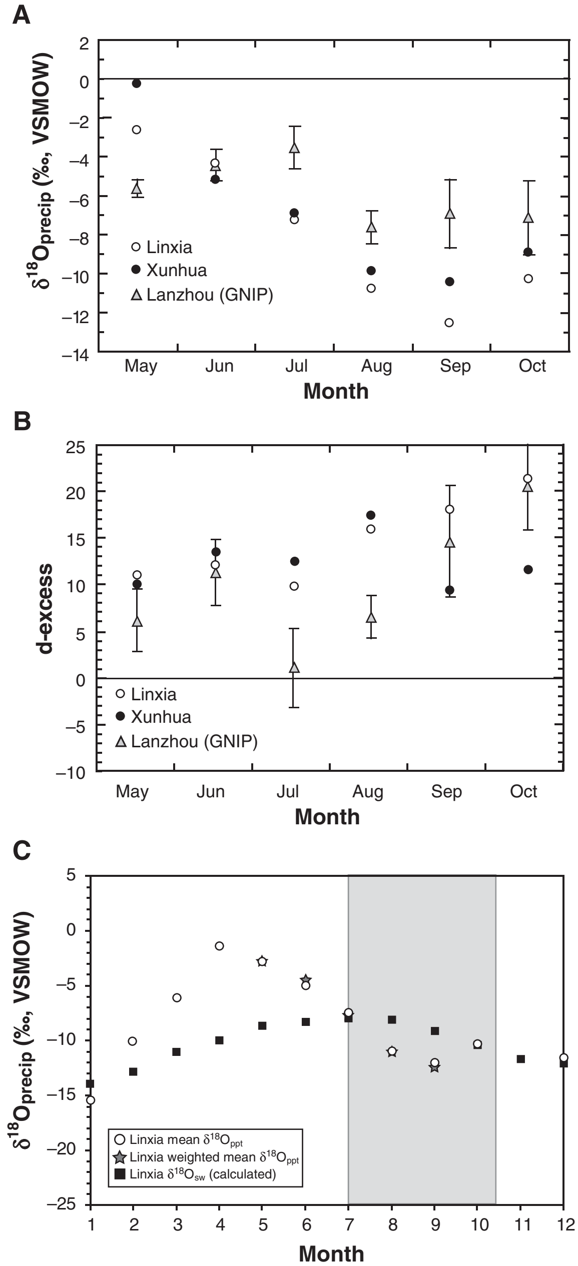

Figure 4. Temporal trends in (A) $\delta^{18}O$ and (B) d-excess for 2007–2008 summertime rainfall. Lanzhou Global Network of Isotopes in Precipitation (GNIP) data are plotted as 6 yr regional mean. (C) Comparison of modern rainfall $\delta^{18}O$ to soil water $\delta^{18}O$. The $\delta^{18}O_{sw}$ is calculated from Quaternary soil carbonates using the mean monthly temperature and the temperature-dependent fractionation equations of Kim and O'Neil (1997). Measured Quaternary soil carbonate $\delta^{18}O$ = –9.0‰ (Vienna Peedee belemnite [VPDB]). Error bars represent the 1σ standard error of the means. Gray interval highlights the late summer months when soil carbonate is expected to precipitate. VSMOW—Vienna standard mean ocean water.

26.6/41.0 cm/yr (the values left of the slash are annual total rainfall for 2007 and values right of the slash are for 2008) (Table DR1 [see footnote 1]). The majority of this rainfall (>75%) occurs during the summer (May–September) and is associated with southeasterly wind directions (Fig. DR2 [see footnote 1]) indicating that sources of summer storms in NE Tibet are from the east and southeast.

In addition to differences in modern rainfall amount, differences are also observed in the average stable isotope composition ($\delta^{18}O_{rw}$ and δD_{rw}) ±1 standard error of rainfall across the Jishi Shan. Monthly mean $\delta^{18}O_{rw}$ (and δD_{rw}) values from 2007 to 2008 rainfall in the Xunhua basin ranged from –0.5‰ to –12.6‰ (+5.8‰ to –115.7‰) with a summer precipitation weighted mean of –6.5‰ ± 1.8‰ (–38.9‰ ± 13.8) (May–September), while those in Linxia ranged from –1.4‰ to –15.3‰ (–10.5‰ to –115.3‰), with a weighted mean summer value of –7.7‰ ± 1.9‰ (–45.7‰ ± 13.1‰) (May–September; Table 1). Both localities show $\delta^{18}O_{rw}$ and δD_{rw} values of precipitation that tend to deplete throughout the summer (Fig. 4A), as expected from Rayleigh distillation models. However, contrary to simple Rayleigh-type distillation models, in which a vapor mass becomes progressively depleted along its rainout path, the $\delta^{18}O_{rw}$ values of Xunhua summer precipitation are, on average, 1.2‰ (δD = 6.8‰) more positive than Linxia precipitation. This downwind difference suggests that rainwater in the Xunhua basin is evaporatively enriched relative to Linxia and therefore that the Xunhua basin is more arid than the Linxia basin; this inference is consistent with the 30% decrease in rainfall in the Xunhua basin. Because of the close proximity of the two basins, this difference in aridity is most easily explained by the presence of a rain shadow in the lee of the Jishi Shan.

The regional δD-$\delta^{18}O$ relationship for monthly rainwater from Linxia and Xunhua and the long-term monthly average from Lanzhou (Fig. 5) form a local meteoric water line (LMWL) defined by:

$$\delta D = 7.1 \times \delta^{18}O + 5.0.$$

The LMWL has a lower slope than Craig's (1961) global meteoric water line (GMWL; $\delta D = 8 \times \delta^{18}O + 10$), which indicates nonequilibrium fractionation during rainfall events within an air column below saturation (<100% relative humidity) (Gonfiantini et al., 1986).

The deuterium excess (d-excess), *d*, as defined by Dansgaard (1964), calculated by,

$$d = \delta D - 8 \times \delta^{18}O,$$

is based on the global relationship between deuterium and ^{18}O composition in freshwater. Values of d-excess can be used to track processes such as nonequilibrium evaporation (at <100% relative humidity) and recycling of water vapor via surface-water evaporation (Gat, 1996). Monthly mean values of d-excess from 2007 to 2008 rainfall in the Xunhua basin (Table 1) ranged from –14.9‰ to 14.5‰, with a summertime (May–September) precipitation weighted mean of 13.4‰ (±1.2). In the Linxia basin d-excess values ranged from –0.9‰ to 22.5‰, with a summertime precipitation weighted mean of 13.5‰ (±1.6). Individual monthly mean d-excess values are generally higher for the Linxia basin than those for the Xunhua basin (Fig. 4B; Table 1). Over the 6 yr of data for Lanzhou during the same months, precipitation weighted d-excess values were much lower for Lanzhou, ranging between 1.2‰ and 14.8‰ (Fig. 4B; Table 1).

The $\delta^{18}O_c$ composition of soil carbonates is ultimately derived from rainfall that infiltrates the soil, with some modification resulting from evaporative enrichment of ^{18}O within the soil. In extremely arid settings, extensive evaporation can increase the $\delta^{18}O_c$ value of soil water and soil carbonate on the order of 10‰

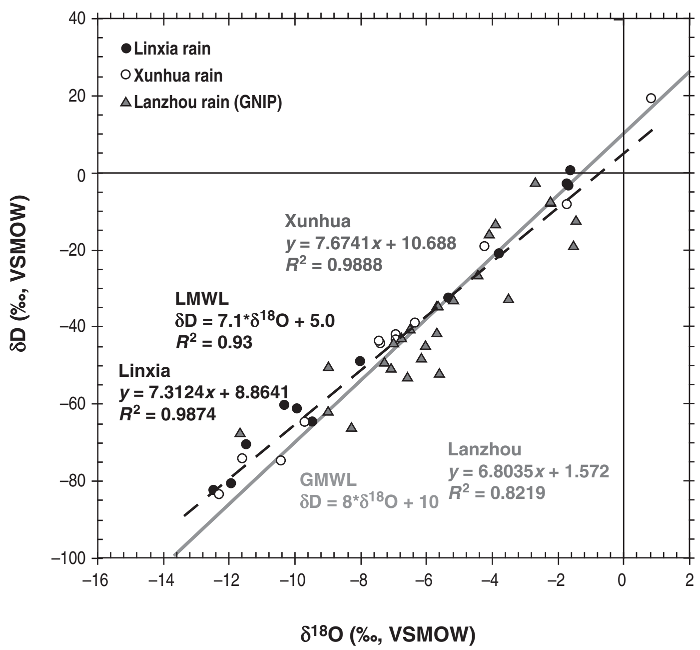

Figure 5. $\delta^{18}O$ versus δD plot of monthly precipitation for summer 2007–2008 rainfall in Linxia and Xunhua basins (May–October). Monthly mean data are weighted based on monthly precipitation amount. Data for Lanzhou precipitation are from Global Network of Isotopes in Precipication (GNIP) and span six years (1985, 1986, 1996–1999). LMWL—local meteoric water line; GMWL—Global meteoric water line.

(e.g., Liu et al., 1996; Hsieh et al., 1998). Comparison between soil carbonate and local rainfall from a range of climate settings indicates that carbonate sampled from deeper parts of the soil profile (greater than ~30 cm) in climates that receive more than 30–35 cm/yr of rainfall reflects similar $\delta^{18}O$ values to local rainfall, whereas lower amounts of annual rainfall may overestimate $\delta^{18}O$ values as a result of evaporation of soil water (Quade et al., 2007). To compare the isotopic composition of rainwater to that of soil carbonate, we need to account for the temperature-dependent fractionation between water and carbonate. The ^{18}O composition of modern soil water ($\delta^{18}O_{sw}$) can be calculated from the $\delta^{18}O_{sc}$ value of modern soil carbonate using the temperature-dependent fractionation equations of Kim and O'Neil (1997), if the temperature of carbonate precipitation is known. We used the mean monthly air temperature along with measured $\delta^{18}O_{sc}$ values of Quaternary soil carbonates to calculate a $\delta^{18}O_{sw}$ value of modern soil water (Fig. 4C). Because soil carbonates precipitate from soil water as the soil dries (and becomes supersaturated with carbonate), we anticipate that the timing of carbonate precipitation in NE Tibet occurs between the peak and the end of the summer rainy season (typically July to October; Table 1), when plants are actively transpiring and soil water is evaporating. We note, however, that a recent study in central New Mexico suggests that pedogenic carbonate may also precipitate in late spring (May) (Breecker et al., 2009). Our temperature-based estimates for the $\delta^{18}O_{sw}$ value of soil water are on average 3.2‰ higher than those of modern rainfall in August and September, but nearly identical in July and October. The overlapping to slightly positive soil water estimates relative to local rainfall in the Linxia basin suggest that soils in this setting experience an average 1‰–2‰ increase in $\delta^{18}O_{sc}$ values associated with evaporative enrichment of ^{18}O. This enrichment agrees with observations from other regions that receive a similar amount of annual rainfall (Quade et al., 2007). We note that our measurements of modern rainfall span only 2 yr, whereas the accumulation of soil carbonate may integrate climate conditions over several thousands of years or longer. Assuming that this relationship between soil carbonate and meteoric water applies to the past, inferences about paleo–meteoric water, and thus paleoclimate, can be made from the analysis of paleocarbonate materials.

Pedogenic Carbonates and Lacustrine Micrite Results

Calcareous minerals that precipitated in both lacustrine and pedogenic environments are considered to be faithful recorders of local to regional climate conditions. The prevalence of these materials in Neogene strata across NE Tibet allows us to use stable isotope analysis to evaluate paleoclimate and its relationship to local- and regional-scale tectonics. Because the Linxia basin is upwind of the Xunhua basin, Linxia's carbonate $\delta^{18}O_c$ and $\delta^{13}C_c$ composition can be used as a baseline to which Xunhua basin carbonates can be compared.

Oxygen isotope values in both lacustrine micrites and pedogenic carbonates are ultimately controlled by the composition of meteoric water. Pedogenic carbonates reflect local rainfall that percolates through the soil profile (see previous results section), whereas lake waters reflect a regional average of precipitation and groundwater from across the entire catchment. Although the two isotopic values are related to local rainfall, they are not directly comparable due to potential differences in source, residence time, and degree of evaporation (Quade et al., 2007). Furthermore, evaporation may cause an increase in the $\delta^{18}O$ values of surface and near-surface waters. This effect is most pronounced in closed-basin lakes (no outflow) where water is lost by infiltration and evaporation (Talbot, 1990), as compared to open lakes and paleosols.

The $\delta^{13}C$ value obtained from pedogenic soil carbonate samples ($\delta^{13}C_c$) represents the amount, type, and seasonality of local vegetation (Cerling and Quade, 1993; Wang and Follmer, 1998). In general, $\delta^{13}C_c$ values of ~+2‰ represent a dominantly C_4 plant community, whereas values ~–12‰ represent a dominantly C_3 plant community. Values between –7‰ and +2‰ represent a mixed community, water-stressed vegetation, or both (Cerling and Quade, 1993; Ehleringer and Cerling, 2002). Plants using the C_4 photosynthetic pathway significantly expanded their global range after ca. 8 Ma (Cerling et al., 1993), but this expansion is not evident in central China until ca. 4–2 Ma (Ding and Yang, 2000; Wang and Deng, 2005). This timing is important for two reasons:

(1) It limits possible paleoenvironmental interpretations in that variations in $\delta^{13}C_c$ must be due to either water stress or the presence of C_4 grasses (Cerling and Quade, 1993; Wang and Follmer, 1998; Ehleringer and Cerling, 2002).

(2) It helps to place constraints on the chronology of the sediments in the Xunhua basin, which is in close proximity to Linxia basin where C_4 plants appeared at ca. 3–2 Ma (Dettman et al., 2003; Wang and Deng, 2005).

Carbon isotopes in lacustrine micrites reflect the biologic productivity of a lake (McKenzie et al., 1985; Talbot, 1990). Increased photosynthesis in the lake preferentially removes ^{12}C from the lake water, leaving the remaining water enriched in ^{13}C and resulting in an increase in the $\delta^{13}C_c$ values of carbonates. Lakes tend to precipitate carbonate in late spring through summer (McKenzie et al., 1985; Drummond et al., 1995) when temperatures are at their warmest and ^{13}C is most enriched.

In total, 105 samples of pedogenic soil carbonate and calcareous micrite were collected from the 530-m-thick lower Xunhua section plus an additional 140 samples from the 940-m-thick upper Xunhua section, resulting in an average sampling interval of ~6 m/sample. Sampling density was highest in the lacustrine and marginal lacustrine deposits of the upper Xunhua section (~3 and ~5 m/sample, respectively) and lowest in the coarser-grained fluvial and alluvial deposits at the top of the upper Xunhua section (~10.7 and ~7.0 m/sample, respectively).

Paleosol carbonate nodules and calcareous cement from the lower Xunhua section yielded $\delta^{18}O_c$ values averaging –10.7‰ (n = 56; σ = 1.3‰), which trend toward more negative values in the lowest 200 m of the section and then become gradually more positive. Lacustrine micrites from the lower Xunhua section yielded –9.7‰ (n = 27, σ = 1.2‰), which trend to more positive values with increased variability near the top of the lower section. Upper Xunhua section lacustrine micrites yielded highly variable $\delta^{18}O_c$ values that average –5.5‰ (n = 38, σ = 1.9‰). Paleosol carbonate nodules and calcareous cement yielded much more consistent, but lower, $\delta^{18}O_c$ values that average –7.7‰ (n = 95, σ = 0.99‰) (Fig. 6). Near the top of the upper Xunhua section (~850 m, Fig. 6), $\delta^{18}O_c$ values appear to increase in variability.

Across the lacustrine to marginal lacustrine facies boundary (located at 170 m in the upper Xunhua section in Figs. 2 and 5), $\delta^{13}C_c$ values have an overall average of –3.4‰, but they gradually decrease by 4‰ (from ~–2‰ to ~–6‰) over 193 m of section (n = 43; R^2 = 0.54). Above the marginal lacustrine to fluvial facies boundary at ~220 m, $\delta^{13}C_c$ values of pedogenic carbonates are relatively constant, with an average of –6.2‰ (n = 95, σ = 0.9‰) (Fig. 6).

Covariability of δ18O and δ13C

Covariance in $\delta^{18}O_c$ and $\delta^{13}C_c$ within lacustrine micrites is a function of the degree of basin closure (outflow versus evaporation) (Talbot, 1990; Drummond et al., 1995; Li and Ku, 1997). In closed lake basins, increasing aridity leads to increased evaporation and to falling lake levels, which, in turn, result in higher lake-water $\delta^{18}O$ values, increased biologic productivity, and higher $\delta^{13}C$ values. Therefore, basins with high correlation between $\delta^{18}O_c$ and $\delta^{13}C_c$ (correlation coefficient [r] >0.7) are interpreted as originating from closed basins (Talbot, 1990; Drummond et al., 1995; Li and Ku, 1997). Cross-plots (Fig. DR3 [see footnote 1]) of $\delta^{18}O_c$ versus $\delta^{13}C_c$ for lacustrine samples within the lower (n = 27; r = 0.460) and upper (n = 38; r = 0.117) Xunhua sections show generally poor covariance and relatively low $\delta^{18}O_c$ and $\delta^{13}C_c$ values, indicating shorter residence times and an overall open lake system (Talbot, 1994). However, samples from the uppermost 100 m of the lower Xunhua section (n = 7) and the uppermost 30 m of lacustrine sediments in the upper section (n = 6), as well as a narrow interval within the upper section (n = 6), do correlate (r = 0.83, 0.89, and 0.90, respectively), suggesting that the Xunhua basin was intermittently hydrologically closed.

ANALYSIS OF DIAGENESIS

Isotopic analyses of 10 diagenetically altered samples containing sparry calcite that infills dissolution vugs yielded $\delta^{18}O$ values averaging –10.4‰ (σ = 0.7‰) (Fig. 6). A t-test shows that the $\delta^{18}O$ values of the diagenetically altered samples are significantly different from the nonaltered samples, which average –7.7‰ (t = 11.161, p < 0.05). The more negative $\delta^{18}O$ values of altered samples (–2.7‰ on average) indicate that the $\delta^{18}O$ composition of diagenetic fluids was either more negative or that diagenetic alteration occurred at higher temperatures, perhaps associated with burial. Given that nonaltered samples show significantly different $\delta^{18}O$ values, we infer that they reflect the meteoric/soil water from which the carbonate precipitated.

PALEOMAGNETIC RESULTS

The paleomagnetism of a stratigraphic succession, when both reliably recorded by fine-grained lithologies as well as unequivocally determined from laboratory demagnetization measurements, can provide a precise chronology of deposition when correlated to the geomagnetic polarity time scale (GPTS). Magnetostratigraphic studies of the Linxia (Fang et al., 2003), Guide (Fang et al., 2005), and Xining (Dai et al., 2006) basins adjacent to Xunhua basin highlight the potential for Xunhua magnetostratigraphy to provide useful constraints on the timing of environmental change in Xunhua basin.

We progressively demagnetized Xunhua paleomagnetic specimens throughout the upper and lower Xunhua sections to track the evolution of the local magnetic field as recorded in Xunhua strata. The intensity of the natural remanent magnetism (NRM) for Xunhua specimens is typically ~10^{-5}–10^{-6} emu/cm^3. After liquid-N_2 treatment, specimens typically displayed a drop in magnetic intensity of <10%, indicating that no significant remanence was carried by multidomain magnetite or hematite. Our stepwise demagnetization procedure clearly resolved three components—a low-coercivity, low-temperature component, an intermediate-temperature component, and a high-temperature component (Fig. DR4 [see footnote 1]). The low-temperature component is typically removed by 100 G (AF) or 150 °C (thermal), but sometimes not until 450 °C. It does not usually decay toward the origin and is interpreted to be a viscous overprint.

The characteristic remanent magnetization (ChRM) includes intermediate- and high-temperature components: the former encompasses the demagnetization steps between 100 G (or sometimes a higher low-temperature component end point) and ~580 °C, whereas the latter encompasses all thermal steps >~580 °C. In most circumstances, both decay toward the origin, show stable behavior, and give similar directions (Fig. DR4A [see footnote 1]). This demagnetization behavior occurs in superposed samples of opposite polarity. In rare cases, however, stable intermediate-temperature component behavior is followed by unstable high-temperature component behavior (Fig. DR4B [see footnote 1]). In this circumstance, our ChRM direction is defined solely by the intermediate component.

Complete unblocking of the high-temperature component by 680 °C indicates a hematite carrier, although a magnetite carrier is also suggested by a small drop in remanence at ~580 °C in many samples. Coercivity spectrum analysis of isothermal remanent magnetism (IRM; Fig. DR5 [see footnote 1]) shows a range of behavior. At one extreme, gradual, continual acquisition of an isothermal remanent magnetism with increasing field strength is consistent with hematite as the primary carrier of magnetism (Butler, 1992). At the other extreme, saturation of an isothermal remanent magnetism at low field strengths (<200 mT) is consistent with (titano-) magnetite as the primary carrier of magnetism. Typical behavior for Xunhua specimens lies somewhere between these extremes, with initial, rapid isothermal remanent magnetism acquisition followed by gradual isothermal remanent magnetism acquisition—a pattern indicating that both magnetite and hematite are the primary carriers of magnetism.

ChRM directions were determined for each specimen using principal component analysis

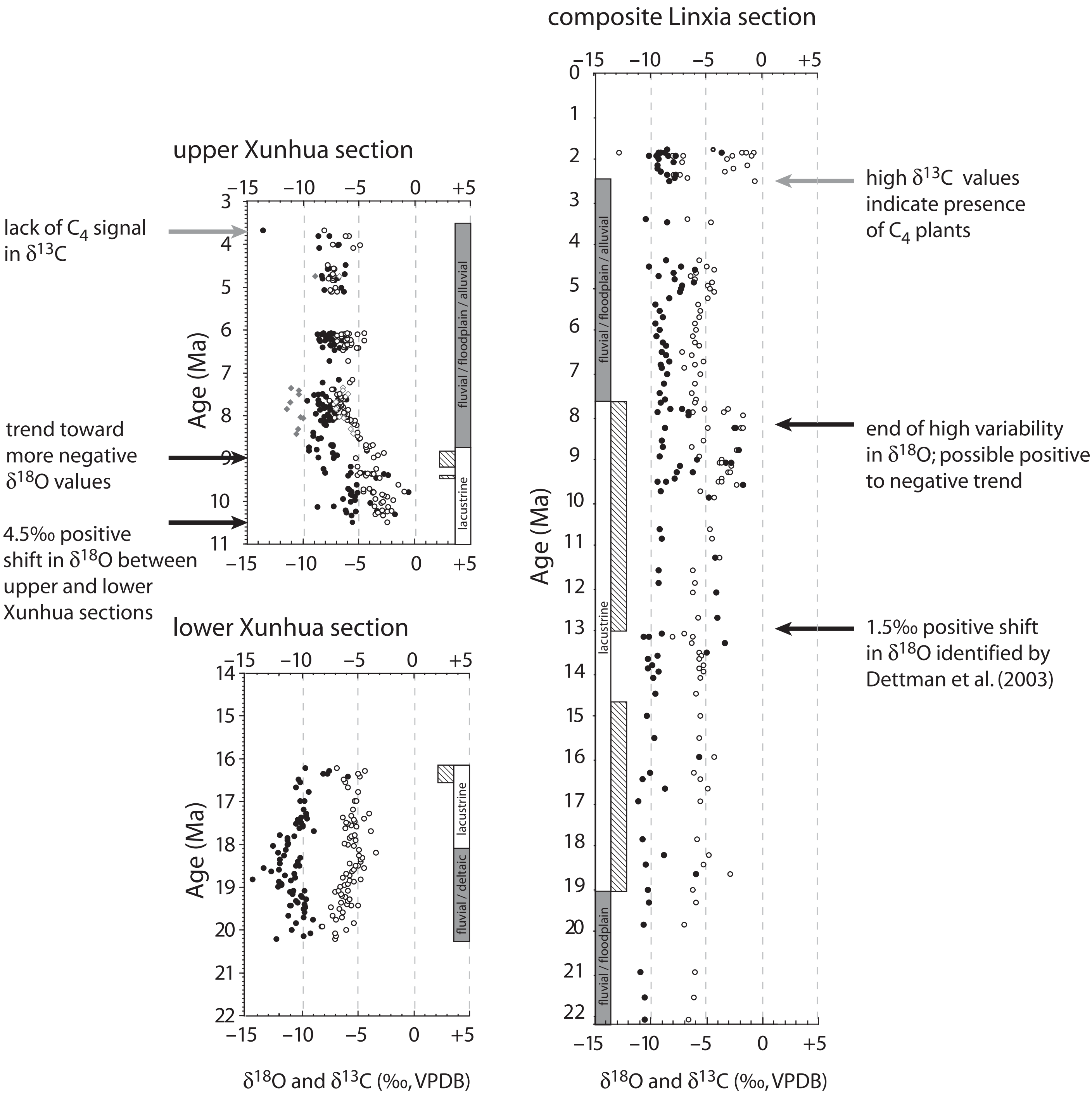

Figure 6. Isotopic correlation of the Xunhua and Linxia sections. Filled circles—$\delta^{18}O$; open circles—$\delta^{13}C$. Filled diamonds—$\delta^{18}O$ of diagenetically altered samples; open diamonds—$\delta^{13}C$ of diagenetically altered samples. Hatched bars indicate periods of closed lake basin conditions as determined by covariance analysis. Linxia stable isotope record from Dettmann et al. (2003).

(Kirschvink, 1980) as implemented in PaleoMag 3.1.0 b1 (Jones, 2002), typically from 11 points (minimum 3 points, maximum 20) from the stable intermediate- and/or high-temperature components. The origin was included only if the demagnetization path decayed toward it. A virtual geomagnetic pole (VGP) was then calculated; their latitudes denote either a normal or reversed polarity of the magnetization of the specimen. Specimens with a noisy or ambiguous orthogonal demagnetization diagram or a maximum angular deviation (MAD) >15° were excluded from further analysis; this removed 20% of the measured specimens. The average deviation for resulting specimens is 8°. A positive reversal test suggests that the average normal and reversed poles are antipodal, passing at C quality (McFadden and McElhinny, 1990), whereas a positive fold test suggests that the data are more tightly clustered (in antipodal pole directions) when corrected for stratigraphic bedding orientation (Tauxe, 1998). The positive reversal and fold tests (Fig. DR6 [see footnote 1]) attest to the general reliability of our demagnetization data in defining the depositional remanence.

AGE CONSTRAINTS

Lithostratigraphic Correlation

Even though the Xunhua and Linxia basins are currently separated from one another, both basins have similar sediment sources and were likely subjected to similar regional climatic conditions over their depositional histories, and as such we would expect to find similar facies in each basin at approximately the same time. The Xunhua sections are flanked by two magnetostratigraphically dated sections, Linxia (Fang et al., 2003) to the east and Guide (Fang et al., 2005) to the west. Lithostratigraphic correlation of the well-dated sections from Linxia and Guide to the Xunhua basin sediments (Fig. 2) provides some preliminary age constraints for the Xunhua sections (Table 2). All three sections (Linxia, Xunhua, and Guide) coarsen upward from lacustrine micrites to cobble conglomerates and contain remarkably similar lithologies (Figs. 2 and 3), though Linxia accumulation rates (~60 m/m.y.) are nearly half of those in Xunhua and Guide (~120 and 140 m/m.y.). A facies change from fluvial or floodplain environments to marginal lacustrine or lacustrine environments near the top of the lower Xunhua section (at 270 m in Fig. 2) and the pervasive presence of gypsum veins above this boundary suggest possible correlations to either (1) the Zhongzhuang Formation or (2) the Dongxiang Formation found in the Linxia basin (Fang et al., 2003). Gypsum-rich marginal lacustrine or lacustrine deposits are also found at the base of the upper Xunhua section (Figs. 2 and 3E). Assuming nearly constant sediment accumulation rates between the two Xunhua sections, the 700 to 800 m gap between them should represent ~5 m.y., such that correlation of the top of the lower Xunhua section to the Zhongzhuang Formation and the base of the upper section to the Dongxiang Formation in Linxia seems most plausible.

The first appearance of obvious fluvial deposits and the cessation of gypsum precipitation within the Linxia and Guide sections best define the boundary between lacustrine and fluvial environments. This boundary is found near the top of the Dongxiang Formation at ca. 8.75 Ma in the Linxia basin (Fang et al., 2003) and within the Ashigong Formation in the Guide basin at ca. 10.2 Ma (Fang et al., 2005). In the Guide section, however, fluvially deposited sandstone is not common prior to ca. 8.75 Ma. Placing the facies boundary at ca. 8.75 Ma, instead of at the first occurrence of fluvial deposits, yields a nearly synchronous boundary in the Linxia and Guide sections. Because these two sections lie on either side of the Xunhua basin, this boundary therefore suggests a constraint on the age of fluvial deposits near the base of the upper Xunhua section (Fig. 2; Table 2).

Additionally, a cobble conglomerate identified as the Jishi Formation by Fang et al. (2003) in the Linxia basin and as the Ganjia Formation by Fang et al. (2005) in the Guide basin spans 3.6–2.6 Ma in both locations. A similar conglomeratic unit found in Xunhua (Fig. 2) provides a correlation point at the top of the upper Xunhua section (Table 2).

Chemostratigraphic Correlation

Carbon Isotopes

Whereas no absolute date has been obtained for the top of the Xunhua section, carbon isotope values from paleosols near the top of the section can be used to infer an upper age limit that is independent of lithologic correlation. The Linxia $\delta^{13}C$ stratigraphic record contains relatively positive $\delta^{13}C_c$ values (maximum $\delta^{13}C = -0.67‰$) at ca. 2.53 Ma (Dettman et al., 2003) (Fig. 6). Additionally, fossil tooth enamel of Neogene mammals from the Linxia basin shows a similar increase in $\delta^{13}C$ values at 2–3 Ma (Wang and Deng, 2005). These data indicate that C_4 plants had expanded into the region and made up the dominant biomass by 2–3 Ma. Similarly positive values are not seen in the Xunhua record (maximum $\delta^{13}C$ ~–4.5‰) (Fig. 6), suggesting that C_4 plants may have been present, but were not the dominant biomass. Whereas expansion of C_4 plants across Asia was not an instantaneous process, it is unlikely that the expansion of C_4 plants reached Linxia, but not Xunhua (only ~50 km away). Therefore, the lack of a significant C_4 signal in the Xunhua paleosols conservatively limits the youngest sedimentary rocks in our upper section to >2.5 Ma.

Oxygen Isotopes

Oxygen isotope values from soil carbonates in both Xunhua and Linxia (Dettman et al., 2003) maintain nearly invariant values, which allow for an interbasin comparison of mean values. However, lacustrine carbonates exhibit much more variable $\delta^{18}O_c$ values (due to evaporative enrichment of lake waters), from which only the most negative (but nondiagenetic) values are likely to represent local rainfall compositions.

Comparisons of oxygen isotope records from the upper Xunhua section with those from Linxia (Dettman et al., 2003) show that both records maintain consistent values within paleosol carbonates from the fluvial and marginal lacustrine environments. These trends become much more variable near the marginal lacustrine to lacustrine boundary (Fig. 6). This change in isotope variability is most likely related to the variable influence of evaporatively enriched lake water and rainwater that infiltrated lake-margin paleosols. In addition to the change in isotopic variability, a 2.2‰ offset to more negative oxygen isotope values (from –5.5‰ to –7.7‰) is also observed at this same position in the upper Xunhua record. A similar offset in the Linxia record is less obvious, but may exist between ca. 8.5 Ma and ca. 7.95 Ma. Although we cannot be certain that this transition to fluvial/floodplain settings occurs simultaneously in Linxia and Xunhua, the observation that Guide basin to the west of Xunhua shows a similar

TABLE 2. SUMMARY TABLE OF CONSTRAINTS USED IN PALEOMAGNETIC CORRELATION

Tie point	Age (Ma)	Uncertainty (m.y.)	Rationale
a (top of section)	3	+1.5/–0.5	(I) Lack of C4 signal at the top of the Xunhua section suggests that this point must be older than regional C4 plant expansion seen in Linxia at 2–3 Ma (Wang and Deng, 2005; Ding and Yang, 2000). (II) Top of section is within cobble conglomerate (Jishi Formation equivalent) and therefore should be older than 2.6 Ma (see tie point "b").
b (base of conglomerate)	3.6	+0.9/–0.02	Presence of cobble to boulder conglomerate that is lithologically similar to the Jishi conglomerate (2.6–3.6 Ma; an unconformity exists from 3.6 to 4.5 Ma; Fang et al., 2003) in the Linxia basin and the Ganjia conglomerate (2.58–3.58 Ma; Fang et al., 2005) in the Guide basin.
c (lacustrine to fluvial transition)	8.5	+0.5/–0.5	First presence of obvious fluvial deposits. Correlates paleomagnetic time scales established by Fang et al. (2003, 2005) to our own measured section in the Guide basin and to the published section in the Linxia basin (Fang et al., 2003).
d (climate reorganization)	12–13		Dettman et al. (2003) interpreted a 1.5‰ positive shift in Linxia $\delta^{18}O$ values at 12–13 Ma to be the result of a regional climate reorganization. This shift is not observed within either the upper or lower Xunhua records, but is evident between them. (Upper section exhibits $\delta^{18}O$ values that are more positive than those in the lower section.)

timing for this facies transition (ca. 8.7–9 Ma) suggests that a regional transition from lacustrine to fluvial depositional environments occurred at ca. 8.5 Ma. Therefore, we use this generally consistent chemostratigraphic and lithostratigraphic age constraint as a tie point for our magnetostratigraphic correlation.

A second $\delta^{18}O_c$ offset exists between the upper and lower Xunhua sections. At the top of the lower section, lacustrine carbonates have an average value of –9.9‰, whereas average values for lacustrine carbonates at the base of the upper section average –5.5‰. Although smaller in magnitude, Dettman et al. (2003) documented a similar shift from negative values (–10.5‰) to relatively more positive ones (–9‰) in the Linxia record at the base of the Dongxiang Formation at ca. 13 Ma. If correlative, the offset between sections in Xunhua suggests that the base of the upper section is younger than 13 Ma and that the top of the lower section is older than 13 Ma. However, as discussed subsequently, the large-magnitude $\delta^{18}O_c$ shift between the upper and lower sections in Xunhua basin is likely a cumulative effect that convolves a regional change together with the emergence of the Jishi Shan.

Magnetostratigraphic Correlation

In an effort to constrain the chronology of deposition as precisely as possible within the framework of the litho- and chemostratigraphic tie points (Table 2), we established a detailed Xunhua magnetostratigraphy. Twenty normal polarity and 20 reversed polarity magnetozones were identified on the two Xunhua sections, labeled N1–15 for the upper section and N16–20 for the lower section (Fig. 7). Two or more specimens of the same polarity define each magnetozone. Additionally, six minor,

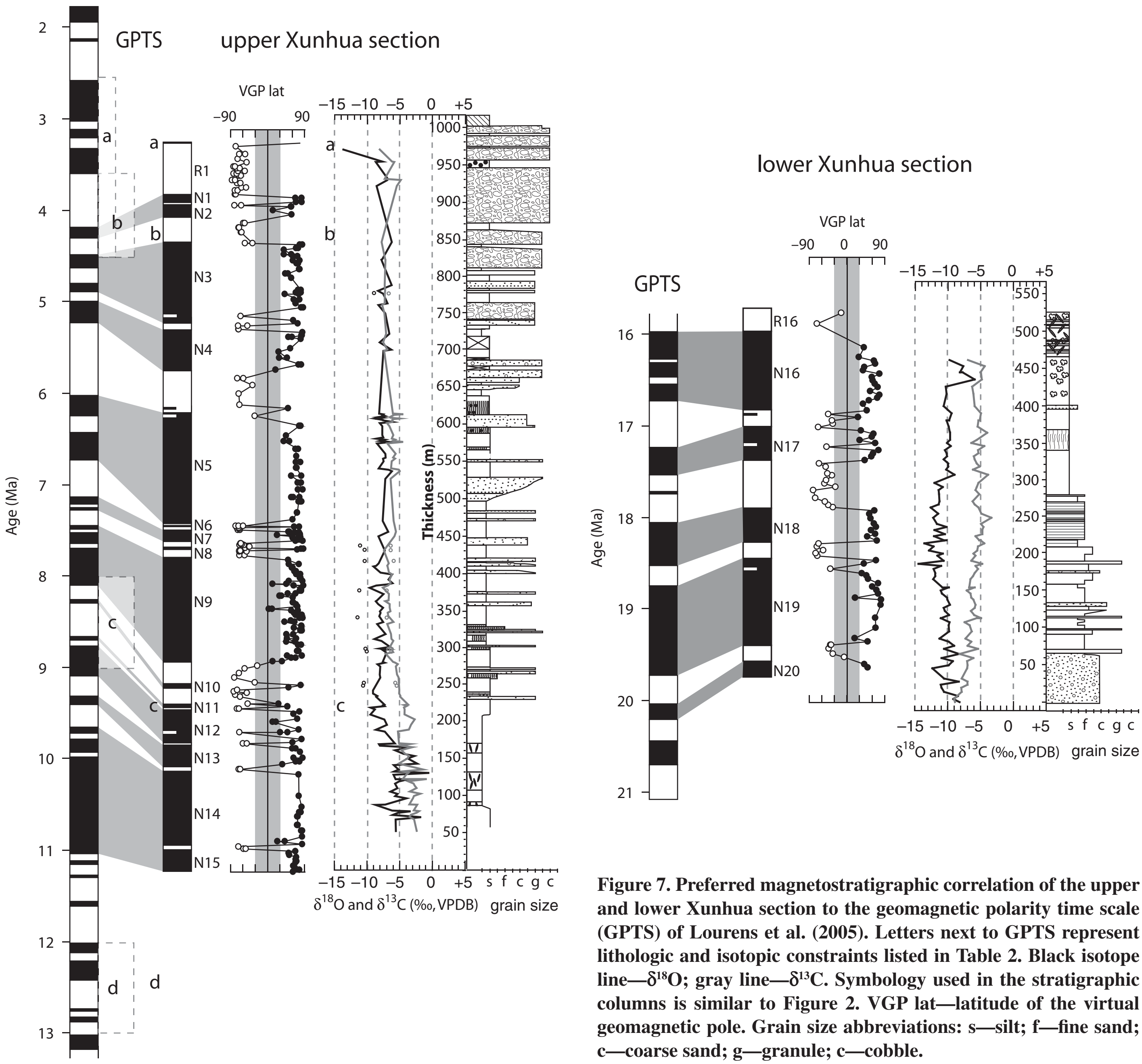

Figure 7. Preferred magnetostratigraphic correlation of the upper and lower Xunhua section to the geomagnetic polarity time scale (GPTS) of Lourens et al. (2005). Letters next to GPTS represent lithologic and isotopic constraints listed in Table 2. Black isotope line—δ^{18}O; gray line—δ^{13}C. Symbology used in the stratigraphic columns is similar to Figure 2. VGP lat—latitude of the virtual geomagnetic pole. Grain size abbreviations: s—silt; f—fine sand; c—coarse sand; g—granule; c—cobble.

questionable polarity zones that are defined by only one specimen are noted with half-width bars. A jackknife resampling attests to the robustness of the magnetostratigraphic data set, returning a value of –0.0811, which falls within the recommended range of 0 to –0.5 (Tauxe and Gallet, 1991) (Fig. DR7 [see footnote 1]). A statistical assessment of the number of reversals expected (45) given our sampling density for the periods 3.6–11 Ma and 15.8–20.3 Ma, however, is slightly greater than the actual number of reversals (40) that we detected (Johnson and McGee, 1983), suggesting that we have not recovered the complete magnetostratigraphy. Furthermore, we do not use the more conservative criterion of defining each magnetozone with two or more sites (in part, because each site has multiple specimens) because the resulting magnetostratigraphy has even fewer reversals (30) than expected (45).

An unresolved problem with the interpretation of the magnetostratigraphy of the upper Xunhua section is the ubiquity of normal polarity throughout the section. Normal polarity constitutes 74% of the upper section, even though the geomagnetic polarity time scale (GPTS) is generally ~50% normal polarity on time scales of >5 m.y. throughout the Cenozoic and is 48% normal polarity during the interval from 3.6 to 11 Ma. We reproduced our data from the upper section by running two or more specimens from 84% of the sampling sites, processing each at a different paleomagnetic laboratory. The replicate specimens gave reproducible results, returning the same magnetic polarities for >98% of the pairs. Pairs that disagreed were removed from further consideration.

Although variations in sediment accumulation rate might explain the dominance of normal polarity in the upper section, the implication that normal polarity magnetozones would have significantly higher accumulation rates compared to reversed polarity magnetozones for the duration of 40 magnetozones over several million years is unlikely. One or more unconformities occurring during episodes of reversed polarity also would help explain the ubiquity of normal polarity throughout the upper section, but we found no evidence for such unconformities when measuring the section or mapping in the area.

Another potential explanation for the ubiquity of normal polarity in the upper section is that the ChRM components for a large portion of this section were later overprinted by a normal polarity field. However, this possibility appears unlikely, given the presence of two or more magnetic components of different orientations for most normal polarity specimens, particularly those in the suspiciously long normal polarity magnetozones. For most specimens, our demagnetization procedure identified a low-temperature viscous overprint that was removed before isolating the intermediate- and/or high-temperature component of the ChRM, as opposed to only identifying one magnetic component that is completely overprinted. We can also discount the possibility of a late-stage, high-temperature, hematite overprint for most specimens because demagnetization pathways on orthogonal plots commonly show similar orientations for both the intermediate- and high-temperature components; when unstable high-temperature behavior is present, we avoided complications by limiting our ChRM regression to the intermediate temperatures.

The Xunhua magnetostratigraphy by itself does not provide an unambiguous correlation to the GPTS (Lourens et al., 2005), especially because of the preponderance of normal polarity for which we have no simple explanation. Therefore, we use the four independent litho- and chemostratigraphic tie points discussed earlier (Table 2) to help correlate the magnetostratigraphic sections. We argue that the general pattern of magnetozones is approximately correct (especially for the lower Xunhua section), but their actual relative durations are not well represented (especially for the upper Xunhua section).

In our preferred correlation to the GPTS (Fig. 7), the upper section spans 3.6–11 Ma, and the lower section spans from 15.8 to 20.3 Ma. This correlation honors each of the tie points and minimizes the variability among short-term sediment accumulation rates throughout the section (Fig. DR8 [see footnote 1]). Alternative correlations for the upper section (Fig. DR9 [see footnote1]) violate various tie points and suggest more highly variable short-term sediment accumulation rates (Fig. DR9 [see footnote 1]).

Our preferred correlation for the upper and lower sections suggests a long-term sediment accumulation rate of ~120 m/m.y. for both Xunhua sections. These Xunhua long-term sediment accumulation rates are intermediate between comparable rates in the adjacent Guide (~140 m/m.y.) and Linxia (~60 m/m.y.) basins for the late Miocene–Pliocene portions of those records.

DISCUSSION

Comparison of the stable isotope record in the Xunhua basin to the published record from Linxia (Dettman et al., 2003) can aid in understanding whether the Xunhua and Linxia basins once constituted a larger, unified basin. If the Xunhua and Linxia basins were once linked as a single, larger depocenter, we would expect to find similar records for both lithology and stable isotope composition prior to separation, whereas diverging stable isotope values would reflect the local climatology, hydrology, and depositional environments associated with basin segmentation by the intervening Jishi Shan.

Modern Rainwater

From our analyses of modern rainfall, we identify a downwind 0.8‰–2.0‰ increase in $\delta^{18}O_{rw}$ across the Jishi Shan in the months of July through September (the rainiest three months). Such an increase in $\delta^{18}O_{rw}$ could result from either a higher temperature of condensation (assuming the same vapor mass composition) or an increase in subcloud evaporation of raindrops in the Xunhua basin. Because the 2007–2008 summertime mean monthly temperatures at the Linxia and Xunhua sampling sites were within 3 °C of one another (Table 1), it seems most plausible that the observed $\delta^{18}O_{rw}$ difference is primarily due to subcloud evaporation. Given that water vapor traverses the Jishi Shan before rainout in the Xunhua basin, we assume that the $\delta^{18}O_{rw}$ increase of 0.8‰–2.0‰ reflects the combined effects of altitude (decreases $\delta^{18}O_{rw}$) and subcloud evaporative enrichment (increases $\delta^{18}O_{rw}$), which means that the observed increase across the Jishi Shan is a minimum. For example, using a mean global isotopic vertical gradient of $\delta^{18}O$ with surface elevation of sampling site of 0.28‰/100 m (Poage and Chamberlain, 2001), a vapor mass crossing the 1000–1500 m of relief in Jishi Shan would decrease its $\delta^{18}O$ composition by 2.8‰–4.2‰. Therefore, this value must be offset by an increase of ≥4‰ due to evaporative enrichment to obtain the average observed 1.2‰ difference in $\delta^{18}O_{rw}$ value of summer precipitation. Based on Lee and Fung's (2008) evaporative enrichment model, both small raindrop size and large differences in relative humidity promote evaporative enrichment. Assuming that raindrops smaller than 1 mm typify the Xunhua basin, a significant (20%) to modest (10%) drop in relative humidity (RH) could cause a ≥4‰ increase in $\delta^{18}O_{rw}$ values of rainfall relative to Linxia, a net isotopic enrichment of $\delta^{18}O_{rw}$ that is similar to the observed difference between both the Linxia and Xunhua rainfall and paleosol carbonates. Notably, the measured relative humidity values during the summers of 2007–2008 were consistently 10% higher in Linxia than in Xunhua (Table 1). We also note that d-excess values were 2‰–10‰ higher in the Linxia basin relative to the Xunhua basin during warm season rainfall (July–September; Fig. 4B), supporting the interpretation of increased subcloud evaporation in the Xunhua basin.

Continentality

The "continental effect"—based on equilibrium, Rayleigh-type, distillation—is an overall trend toward depleted isotopic values with increasing distance from the coast (Rozanski et al., 1993). This effect, in the absence of additional water vapor input or changes in air temperature, should dictate that downwind rainwater is depleted relative to an upwind counterpart. Araguás-Araguás et al. (1998) identified the influence of five different air masses over China, but limited availability of data led Araguás-Araguás et al. (1998) to interpret that only the dry central Asian air mass influenced climate within our study area. The results from our modern rainfall study (Table 1) and wind data from Lanzhou (Fig. DR2 [see footnote 1]) show a seasonal rainfall pattern and winds from the east during storms indicative of an eastern water vapor source. Relatively low d-excess values, as compared to the higher values observed in central Asian air masses, appear to confirm this interpretation (Gat et al., 2003). Furthermore, Quade et al. (2007) showed that evaporation may have a significant impact on the $\delta^{18}O$ values of soil water where rainfall is less than 30 cm/yr, such that reconstructions of the isotopic composition of rainfall in arid environments may be in error unless the magnitude of ^{18}O enrichment due to evaporation is taken into account. Our data show that, locally, evaporation may account for $\delta^{18}O$ enrichment in soil water of up to 4.5‰. Based on the observed increase in $\delta^{18}O_{rw}$ on the leeward side of the Jishi Shan, we infer that the $\delta^{18}O_{rw}$ increase identified by Araguás-Araguás et al. (1998) in north-central China, where our study is located, is likely caused by increased evaporative enrichment in this extremely continental setting.

In evaluating paleoclimate records, we assume, based on the distribution of paleotopography that modern vapor trajectories are representative of vapor mass transport in the past. Assuming that the primary control on changes in vapor mass trajectories is the areal extent of high topography associated with the Tibetan Plateau, then new evidence suggesting rapid exhumation of the West Qinling Shan immediately south of the Linxia and Xunhua basins at 45 Ma (Clark et al., 2010) suggests that vapor transport pathways may not have changed appreciably over the past 45 m.y. This assumption is also supported by the relative invariability of the Linxia isotope record back to 29 Ma (Dettman et al., 2003).

Local Tectonics and Climate

Soil Carbonate (2–8.75 Ma)

Pedogenic carbonates from both the Xunhua and Linxia basins maintain consistent soil carbonate $\delta^{18}O$ ($\delta^{18}O_c$) values of –7.7‰ and –9‰, respectively (Fig. 6). The observation that $\delta^{18}O_c$ values are consistently enriched relative to the adjacent Linxia basin indicates that the Xunhua basin has likely been more arid throughout the length of the soil carbonate record (since ca. 8.75 Ma). The 1.3‰ enrichment in Xunhua $\delta^{18}O_c$ values relative to Linxia is consistent with the isotopic differences observed in modern rainfall (precipitation weighted mean = 1.2‰ difference) and could be entirely accounted for by differences in subcloud evaporation (as described previously), or it may reflect a greater magnitude of evaporative enrichment of soil water in Xunhua basin relative to Linxia basin. We interpret this consistent isotopic difference as an indicator of lower relative humidity (i.e., more arid conditions) in Xunhua relative to Linxia basin over the past ~9 m.y. (the time since fluvial/floodplain environments were established). The nearly invariant nature of the Linxia record over the earlier portion of this time interval (Fig. 6) argues for a stable regional climate.

Lacustrine Carbonate (8.75–11 Ma)

Upper Xunhua lacustrine carbonate $\delta^{18}O_c$ values are always more positive than correlative sediments in Linxia, suggesting that the two basins were hydrologically separated throughout the lacustrine record (ca. 11 Ma). The value of the isotopic difference ($\delta^{18}O_{Xunhua}$ minus $\delta^{18}O_{Linxia}$), however, does not remain as consistent in the lacustrine record as it does in the soil carbonate record. Dettman et al. (2003) interpreted the lowest $\delta^{18}O_c$ values in the Linxia lacustrine deposits (–9‰) as open lake conditions that were least affected by evaporative enrichment. Looking exclusively at these baseline values and ignoring shorter-term anomalies, the $\delta^{18}O_c$ values of carbonates from Linxia remain nearly invariant across the marginal lacustrine to fluvial facies transition, whereas in Xunhua deposits, there is a 2.2‰ decrease from an average value of –5.5‰ to –7.7‰ observed across this same boundary (Fig. 6) that reduces the isotopic difference between the two sections ($\delta^{18}O_{Xunhua} - \delta^{18}O_{Linxia}$) from 3.9‰ within the lacustrine interval to only 1.3‰ within the paleosol interval.

The apparently greater aridity suggested by the more positive $\delta^{18}O_c$ values in Xunhua basin paleosols and the hydrologic separation inferred from differences between Xunhua and Linxia lacustrine carbonates through the past 11 m.y. provide the oldest independent evidence for pre–11 Ma growth of the Jishi Shan. Furthermore, this temporal limit implies that the growth strata reported by Fang et al. (2003) and Yuan et al. (2007) beginning at ca. 8 Ma from the Yinchuangou anticline in Linxia basin does not mark the initial surface uplift in the Jishi Shan. Rather, localized basin isolation and aridity observed within the Xunhua basin relative to the Linxia basin at 11 Ma is consistent with deformation and basin isolation by at least 11 Ma.

Lacustrine Carbonates (15.8–16.6 Ma)

In contrast with $\delta^{18}O_c$ values in the upper Xunhua section, which are consistently more positive than corresponding Linxia values, average $\delta^{18}O_c$ values of lacustrine carbonates in the lower Xunhua section (–10‰) match those in the correlative Linxia strata (–10.5‰). The nearly identical $\delta^{18}O_c$ values between basins suggest that the Linxia and Xunhua basins were hydrologically connected at this time. This implies that either significant elevation of the Jishi Shan above the surrounding basins and the resulting hydrologic separation must have occurred after 16 Ma or that a fluvial connection was established between the two basins despite initial growth of the Jishi Shan.

Even with similar $\delta^{18}O_c$ values, the nature of the $\delta^{18}O_c$ signal remains unique between basins. Variability in the lower Xunhua lacustrine deposits is very low ($\sigma^2 = 0.17$, $n = 19$) and yet is quite high in the Zhongzhuang Formation in Linxia ($\sigma^2 = 2.84$, $n = 15$). The difference in variability in these two basins may be related to the degree of basin closure. Based on measurements of covariance between $\delta^{18}O_c$ and $\delta^{13}C_c$ (Fig. DR3 [see footnote 1]), the Xunhua basin was generally hydrologically open throughout this time interval, while Linxia was at least intermittently closed (Dettman et al., 2003). A paleogeographic scenario that could account for these observations would be that the Xunhua basin supplied water to the Linxia basin via a fluvial connection (such as the Yellow River that connects these basins today), while on the downstream end of the system, intermittent closure of the Linxia lake basin led to periodic evaporative enrichment of lake waters.

If the Linxia basin received water from a lake system in Xunhua, the composition of that inflow should have affected the composition of lake waters in Linxia proportionately to the ratio of inflow from Xunhua to total inflow of the lake in Linxia (Davis et al., 2009; Kent-Corson et al., 2009). Because Linxia and Xunhua $\delta^{18}O_c$ values are nearly identical during this time period, it is possible that the Linxia and Xunhua basins were separated by the Jishi Shan prior to 16 Ma and through-flow from Xunhua to Linxia contributed a dominant portion of the water budget for the Linxia basin lake, thereby rendering the composition of the Linxia lake similar to that in the upstream Xunhua basin. To account for the change to more arid conditions in the upstream record after 11 Ma with no accompanying change in the downstream record, either through-flow in Xunhua must have become severely restricted (such that Xunhua water was no longer the dominant source to the Linxia basin), or interbasin differences in aridity must have increased by 11 Ma. Our covariance analysis (Fig. 6; Fig. DR3 [see footnote 1]) does not support a highly restricted outflow from the Xunhua basin after 11 Ma. In addition, evaporite deposits are not prevalent in the Xunhua record prior ca. 16.5 Ma (Fig. 2), which also suggests less arid conditions in the older part of the record. We interpret this to indicate similar climate conditions in both basins prior to ca. 16 Ma and that the Jishi Shan, if present, was a low-standing range at this time.

Soil Carbonates (16.6–20.3 Ma)

Within the soil carbonate record from the lower Xunhua section ($n = 77$), a minor offset is observed in both carbon and oxygen isotope values at 155 m (ca. 19 Ma) (Fig. 6). Average $\delta^{18}O_c$ values decrease from –10‰ to –11.6‰, but average $\delta^{13}C_c$ values increase from –6.8‰ to –5.3‰. The Linxia record does not appear to contain a similar offset (Dettman et al., 2003), possibly because this interval contains very few samples, making comparisons difficult. However, average $\delta^{18}O_c$ values from Linxia (–9.6‰, although most of the $\delta^{18}O_c$ values are closer to –10.5‰) are generally consistent with the values from Xunhua (–10.6‰) during this time interval (Fig. 6), suggesting that the two basins received rainfall of a similar isotopic composition.

The consistency in the $\delta^{18}O_c$ values of both pedogenic and lacustrine carbonates between the Linxia and Xunhua basins over the time period between 20.3 and 15.8 Ma suggests that the basins were hydrologically connected and their climates were similar. Therefore, the Jishi Shan was unlikely to have been a significant topographic feature separating the two basins at this time.

Regional Tectonics and Climate

Increases in $\delta^{18}O_c$ values of carbonate materials interpreted to reflect increased aridity during local mountain building are seen across the northern and northeastern plateau margin during the middle Miocene (Graham et al., 2005; Kent-Corson et al., 2009). Stable isotope compositions of lacustrine, alluvial, paleosol, and fluvial carbonates in the Tarim and Qaidam basins show a trend toward increasing $\delta^{18}O_c$ values (2‰–10‰) during the Neogene (Kent-Corson et al., 2009). The regional distribution of this observed increase in $\delta^{18}O$ values can be interpreted in one of two ways: (1) regional aridification due to changes in global-scale climate or (2) local-scale aridification due to regional tectonic activity.

Recent work on the eastern margin of the Liupan Shan (Fig. 1) documents changes in multiple climate proxy records that are interpreted to reflect cooling and aridification associated with a decrease in the influence of the Asian summer monsoon (and corresponding increase in winter monsoon)(Jiang et al., 2008; Jiang and Ding, 2008, 2010). Although these authors suggest that this unidirectional trend toward cooler, drier climate occurred contemporaneously with the onset of global cooling and aridification associated with a 5 °C global cooling and the expansion of the East Antarctic Ice Sheet (Zachos et al., 2001; Savin et al., 1975), we point out that most of their indicators show that aridification occurred at ca. 12 Ma, whereas global cooling as documented in marine records, occurred prior to 14 Ma (Zachos et al., 2001; Molnar, 2004).

Our results show that aridification in the rain shadow of growing topography is an important factor in determining the composition of rainwater and soil carbonate $\delta^{18}O$. If global climate change was responsible for the increased $\delta^{18}O_c$ values, we would expect to see a synchronous change of nearly equal magnitude in both the Linxia and Xunhua basins and limited interbasin variation. Based on the isotopic differences that developed between the Linxia and Xunhua basins at this time, we interpret the regional increase in $\delta^{18}O_c$ values observed from Tarim basin to Linxia basin in the middle Miocene as the local manifestation of topographic growth across this broad region. Furthermore, we suggest that regional changes in atmospheric circulation associated with topographic growth along the margin of the plateau could account for synchronous aridification at ca. 12 Ma in the Linxia basin (Dettman et al., 2003; Wang and Deng, 2005) and in the Liupan Shan (Jiang et al., 2008; Jiang and Ding, 2008, 2010) that was unrelated to, or supplemental to, the global cooling event prior to 14 Ma.

Deformation of regional-scale structures along the north and northeast margins of the Tibetan Plateau may have begun in the early Eocene. Increased faulting in the West Qinling Shan began ca. 50–45 Ma (Clark et al., 2010) and in Kunlun Shan ca. 35–30 Ma (Mock et al., 1999; Clark et al., 2010). This deformation coincides with a 25° vertical axis rotation of the Xining-Lanzhou region between 45 and 30 Ma (Dupont-Nivet et al., 2004) and is associated with increasing subsidence rates in Xining (from 40 to 30 Ma; Horton et al., 2004) and in Linxia (from 29 to 6 Ma; Fang et al., 2003). Our interpretation of the surface uplift of a smaller range, the Jishi Shan, between 16 and 11 Ma extends ~100 km beyond the West Qinling margin. This deformation was contemporaneous with the growth of topography in the Altyn Shan and along the margins of the Tarim and Qaidam basins, as indicated by apatite fission-track and (U-Th)/He ages that date a transition from low- to high-gradient depositional systems (Ritts et al., 2008) and a regional trend toward increased aridity (Graham et al., 2005; Kent-Corson et al., 2009). Uplift of the Jishi Shan appears to represent the eastern limit of mid-Miocene tectonic activity along the northern plateau margin. Late Miocene exhumation in the northern Qilian Shan, indicated by apatite fission-track (George et al., 2001) and (U-Th)/He thermochronology (Zheng et al., 2010) and in the Liupan Shan indicated by apatite fission-track thermochronology (Zheng et al., 2006), demonstrates that deformation stepped both northward and eastward by ~300 km or more in late Miocene time. This outward step coincides with a decrease in flexural subsidence of the Linxia basin (Fang et al., 2003). The sum of these data indicates that the West Qinling range was the active margin of NE Tibet in Eocene time. By middle to late Miocene time, deformation began to propagate into the low-lying region beyond the West Qinling margin, defining the basins and intervening ranges that make up the region today.

CONCLUSIONS

Our new lithologic, isotopic, and paleomagnetic records from the Xunhua basin suggest that the Xunhua basin contains a sedimentary record that spans the time period of at least 20.3–3.5 Ma. Lacustrine and pedogenic carbonates from the older part of the Xunhua record (20.3–15.8 Ma) show similar $\delta^{18}O_c$ values to lacustrine carbonates in the Linxia basin over this time interval, suggesting a similar climate in both basins and a hydrologic connection between lacustrine environments. An overall shift to more arid conditions occurred between 16 and 11 Ma, with differential aridification across the Jishi Shan such that the Xunhua basin experienced a greater degree of aridification than the Linxia basin. These interbasin differences in paleoclimate conditions have persisted since 11 Ma and are similar to modern interbasin climate differences.

We interpret the evidence to show that increased aridification in the Xunhua basin between 16 and 11 Ma resulted from surface uplift of the Jishi Shan and the subsequent blocking of easterly derived vapor transport pathways. Combined with records of uplift and aridification from the Altyn Shan and Qilian Shan during the middle Miocene, topographic growth in the Jishi Shan suggests active deformation of the northern margin of the Tibetan Plateau from the Tarim basin to the Linxia basin. In addition, evaporative enrichment of rainfall and surface waters due to aridification in the lee of growing topography is likely responsible for the anomalously high $\delta^{18}O_{rw}$ values observed in modern rainfall across northern Tibet.

This study demonstrates that intrabasin comparisons of paleoclimate records from stable isotopes can be used to track the emergence of intervening ranges, such as the Jishi Shan, in regions that show measurable climate differences from basin to basin.

ACKNOWLEDGMENTS

The authors would like to thank Manfred Strecker, Malinda Kent-Corson, and an anonymous reviewer for helpful reviews of the manuscript. This work was supported by National Science Foundation (NSF) grants EAR-0506575 and EAR-0507431 and by National Science Foundation of China (NSFC) grant 40772127. Additional support to Zhicai Wang came from the National Science Foundation of China (40234040, 40772127) and from the State Key Laboratory of Earthquake Dynamics (LED2008A01). Lease acknowledges support from a NSF graduate research fellowship. Funding for the modern rainfall analyses was provided via a Geological Society of America student research grant to Hough. We thank S. Bogue and J. Kirschvink for advice and support during paleomagnetic laboratory work, C. Romanek and D. Dettman for isotopic analyses, J. Smith and P. Higgins for help and advice during stable isotope laboratory work, and J. Smith and J. Minder for assistance in the field. Special thanks go to Zhang Pei-Zhen and colleagues in the China Earthquake Administration who facilitated all aspects of this research.

REFERENCES CITED

Araguás-Araguás, L., Froehlich, K., and Rozanski, K., 1998, Stable isotope composition of precipitation over Southeast Asia: Journal of Geophysical Research, v. 103, no. D22, p. 28,721–28,742, doi: 10.1029/98JD02582.

Bally, A.W., Chou, I.M., Clayton, R., Eugster, H.P., Kidwell, S., Meckel, L.D., Ryder, R.T., Watts, A.B., and Wilson, A.A., 1986, Notes on sedimentary basins in China; report of the American Sedimentary Basins Delegation to the People's Republic of China: U.S. Geological Survey Open-File Report 86-0327, 108 p.

Breecker, D.O., Sharp, Z.D., and McFadden, L.D., 2009, Seasonal bias in the formation and stable isotopic composition of pedogenic carbonate in modern soils from central New Mexico, USA: Geological Society of America Bulletin, v. 121, no. 3–4, p. 630–640.

Butler, R.F., and Butler, R.F., 1992, Paleomagnetism: Magnetic domains to geologic terranes: Boston, Massachusetts, Blackwell Scientific Publications.

Cerling, T.E., and Quade, J., 1993, Stable carbon and oxygen isotopes in soil carbonates, *in* Swart, P.K., Lohmann, K.C., McKenzie, J.A., and Savin, S., eds., Climate Change in Continental Isotopic Records: American Geophysical Union Geophysical Monograph 78, p. 217–231.

Cerling, T.E., Wang, Y., and Quade, J., 1993, Expansion of C4 ecosystems as an indicator of global ecological change in the late Miocene: Nature, v. 361, no. 6410, p. 344–345, doi: 10.1038/361344a0.

Chamberlain, C.P., Poage, M.A., Craw, D., and Reynolds, R.C., 1999, Topographic development of the Southern Alps recorded by the isotopic composition of authigenic clay minerals, South Island, New Zealand: Chemical Geology, v. 155, no. 3–4, p. 279–294, doi: 10.1016/S0009-2541(98)00165-X.

Clark, M.K., Farley, K.A., Zheng, D., Wang, Z., and Duvall, A., 2010, Early Cenozoic faulting of the northern Tibetan Plateau margin from apatite (U-Th)/He ages: Earth and Planetary Science Letters, v. 296, no. 1–2, p. 78–88.

Craig, H., 1961, Isotopic variations in meteoric waters: Science, v. 133, no. 3465, p. 1702–1703, doi: 10.1126/science.133.3465.1702.

Dai, S., Fang, X., Dupont-Nivet, G., Song, C., Gao, J., Krijgsman, W., Langereis, C., and Zhang, W., 2006, Magnetostratigraphy of Cenozoic sediments from the Xining basin: Tectonic implications for the northeastern Tibetan Plateau: Journal of Geophysical Research, v. 111, no. B11, p. B11102, doi: 10.1029/2005JB004187.

Dansgaard, W., 1964, Stable isotopes in precipitation: Tellus (Sweden), v. 16, p. 436–468, doi: 10.1111/j.2153-3490.1964.tb00181.x.

Davis, S.J., Mulch, A., Carroll, A.R., Horton, T.W., and Chamberlain, C.P., 2009, Paleogene landscape evolution of the central North American Cordillera: Developing topography and hydrology in the Laramide foreland: Geological Society of America Bulletin, v. 121, no. 1–2, p. 100.

Dettman, D.L., Fang, X., Garzione, C.N., and Li, J., 2003, Uplift-driven climate change at 12 Ma; a long $\delta^{18}O$ record from the NE margin of the Tibetan Plateau: Earth and Planetary Science Letters, v. 214, no. 1–2, p. 267–277, doi: 10.1016/S0012-821X(03)00383-2.

Ding, Z.L., and Yang, S.L., 2000, C3/C4 vegetation evolution over the last 7.0 Myr in the Chinese Loess Plateau: Evidence from pedogenic carbonate $\delta^{13}C$: Palaeogeography, Palaeoclimatology, Palaeoecology, v. 160, no. 3–4, p. 291–299, doi: 10.1016/S0031-0182(00)00076-6.

Drummond, C.N., Patterson, W.P., and Walker, J.C.G., 1995, Climatic forcing of carbon-oxygen isotopic covariance in temperate-region marl lakes: Geology, v. 23, no. 11, p. 1031–1034, doi: 10.1130/0091-7613(1995)023<1031:CFOCOI>2.3.CO;2.

Dupont-Nivet, G., Horton, B.K., Butler, R.F., Wang, J., Zhou, J., and Waanders, G.L., 2004, Paleogene clockwise tectonic rotation of the Xining-Lanzhou region, northeastern Tibetan Plateau: Journal of Geophysical Research, v. 109, no. 4, p. B04401, doi: 10.1029/2003JB002620.

Ehleringer, J.H., and Cerling, T.E., 2002, C3 and C4 photosynthesis, *in* Mooney, H.A., and Canadell, J.G., eds., Encyclopedia of Global Environmental Change: Chichester, John Wiley & Sons, Ltd., p. 186–190.

Fang, X., Garzione, C., Van der Voo, R., Li, J., and Fan, M., 2003, Flexural subsidence by 29 Ma on the NE edge of Tibet from the magnetostratigraphy of Linxia basin, China: Earth and Planetary Science Letters, v. 210, no. 3–4, p. 545–560, doi: 10.1016/S0012-821X(03)00142-0.

Fang, X., Yan, M., Van der Voo, R., Rea, D.K., Song, C., Pares, J.M., Gao, J., Nie, J., and Dai, S., 2005, Late Cenozoic deformation and uplift of the NE Tibetan Plateau; evidence from high-resolution magnetostratigraphy of the Guide basin, Qinghai Province, China: Geological Society of America Bulletin, v. 117, no. 9–10, p. 1208–1225, doi: 10.1130/B25727.1.

Gansu Bureau of Geology and Mineral Resources (GBGMR), 1989, Regional Geology of Gansu Province (in Chinese with English summary): Beijing, Geological Publishing House, 690 p.

Garzione, C.N., Dettman, D.L., and Horton, B.K., 2004, Carbonate oxygen isotope paleoaltimetry; evaluating the effect of diagenesis on paleoelevation estimates for the Tibetan Plateau: Palaeogeography, Palaeoclimatology, Palaeoecology, v. 212, no. 1–2, p. 119–140.

Garzione, C.N., Ikari, M.J., and Basu, A.R., 2005, Source of Oligocene to Pliocene sedimentary rocks in the Linxia basin in northeastern Tibet from Nd isotopes; implications for tectonic forcing of climate: Geological Society of America Bulletin, v. 117, no. 9–10, p. 1156–1166, doi: 10.1130/B25743.1.

Gat, J.R., 1996, Oxygen and hydrogen isotopes in the hydrologic cycle: Annual Review of Earth and Planetary Sciences, v. 24, p. 225–262, doi: 10.1146/annurev.earth.24.1.225.

Gat, J.R., Klein, B., Kushnir, Y., Roether, W., Wernli, H., Yam, R., and Shemesh, A., 2003, Isotope composition of air moisture over the Mediterranean Sea: An index of the air sea interaction pattern: Tellus, ser. B, Chemical and Physical Meteorology, v. 55, p. 953, doi: 10.1034/j.1600-0889.2003.00081.x.

George, A.D., Marshallsea, S.J., Wyrwoll, K.-H., Jie, C., and Yanchou, L., 2001, Miocene cooling in the northern Qilian Shan, northeastern margin of the Tibetan Plateau, revealed by apatite fission-track and vitrinite-reflectance analysis: Geology, v. 29, no. 10, p. 939–942, doi: 10.1130/0091-7613(2001)029<0939:MCITNQ>2.0.CO;2.

Gonfiantini, R., Fritz, P., and Fontes, J.-C., 1986, Environmental isotopes in lake studies: Amsterdam, Netherlands, Elsevier, p. 113–168.

Graham, S.A., Chamberlain, C.P., Yue, Y., Ritts, B.D., Hanson, A.D., Horton, T.W., Waldbauer, J.R., Poage, M., and Feng, X., 2005, Stable isotope records of Cenozoic climate and topography: Tibetan Plateau and Tarim basin: American Journal of Science, v. 305, no. 2, p. 101–118.

Guo, Z.T., Ruddiman, W.F., Hao, Q.Z., Wu, H.B., Qiao, Y.S., Zhu, R.X., Peng, S.Z., Wei, J.J., Yuan, B.Y., and Liu, T.S., 2002, Onset of Asian desertification by 22 Myr ago inferred from loess deposits in China: Nature, v. 416, no. 6877, p. 159–163, doi: 10.1038/416159a.

Horton, B.K., Dupont-Nivet, G., Zhou, J., Waanders, G.L., Butler, R.F., and Wang, J., 2004, Mesozoic-Cenozoic evolution of the Xining-Minhe and Dangchang basins, northeastern Tibetan Plateau: Magnetostratigraphic and biostratigraphic results: Journal of Geophysical Research, v. 109, no. B04402, p. 1–15, doi: 10.1029/2003JB002913.

Hsieh, J.C.C., Chadwick, O.A., Kelly, E.F., and Savin, S.M., 1998, Oxygen isotopic composition of soil water: Quantifying evaporation and transportation: Geoderma, v. 82, p. 269–293, doi: 10.1016/S0016-7061(97)00105-5.

Hsu, H.H., and Liu, X., 2003, Relationship between the Tibetan Plateau heating and East Asian summer monsoon rainfall: Geophysical Research Letters, v. 30, p. 2066, doi: 10.1029/2003GL017909.

International Atomic Energy Administration/World Meteorological Organization (IAEA/WMO), 2006, Global Network of Isotopes in Precipitation: The GNIP database: http://isohis.iaea.org.

Jiang, H., and Ding, Z., 2008, A 20 Ma pollen record of East Asian summer monsoon evolution from Guyuan, Ningxia, China: Palaeogeography, Palaeoclimatology, Palaeoecology, v. 265, no. 1–2, p. 30–38, doi: 10.1016/j.palaeo.2008.04.016.

Jiang, H., and Ding, Z., 2010, Eolian grain-size signature of the Sikouzi lacustrine sediments (Chinese Loess Plateau): Implications for Neogene evolution of the East Asian winter monsoon: Geological Society of America Bulletin, v. 122, no. 5–6, p. 843–854, doi: 10.1130/B26583.1.

Jiang, H., Ji, J., Gao, L., Tang, Z., and Ding, Z., 2008, Cooling-driven climate change at 12–11 Ma: Multiproxy records from a long fluviolacustrine sequence at Guyuan, Ningxia, China: Palaeogeography, Palaeoclimatology, Palaeoecology, v. 265, no. 1–2, p. 148–158, doi: 10.1016/j.palaeo.2008.05.006.

Johnson, N.M., and McGee, V.E., 1983, Magnetic polarity stratigraphy: Stochastic properties of data, sampling problems, and the evaluation of interpretations: Journal of Geophysical Research, v. 88, p. 1213–1221, doi: 10.1029/JB088iB02p01213.

Jones, C.H., 2002, User-driven Integrated Software Lives: "PaleoMag," Paleomagnetics Analysis on the Macintosh: Computers & Geosciences, v. 28, no. 10, p. 1145–1151, doi: 10.1016/S0098-3004(02)00032-8.

Kent-Corson, M.L., Ritts, B.D., Zhuang, G., Bovet, P.M., Graham, S.A., and Page Chamberlain, C., 2009, Stable isotopic constraints on the tectonic, topographic, and climatic evolution of the northern margin of the Tibetan Plateau: Earth and Planetary Science Letters, v. 282, no. 1–4, p. 158–166, doi: 10.1016/j.epsl.2009.03.011.

Kim, S.T., and O'Neil, J.R., 1997, Equilibrium and nonequilibrium oxygen isotope effects in synthetic carbonates: Geochimica et Cosmochimica Acta, v. 61, p. 3461–3475, doi: 10.1016/S0016-7037(97)00169-5.

Kirschvink, J.L., 1980, The least-squares line and plane and the analysis of paleomagnetic data: Geophysical Journal of the Royal Astronomical Society, v. 62, p. 699–718.

Kirschvink, J.L., Kopp, R.E., Raub, T.D., Baumgartner, C.T., and Holt, J.W., 2008, Rapid, precise, and high-sensitivity acquisition of paleomagnetic and rock-magnetic data: Development of a low-noise automatic sample changing system for superconducting rock magnetometers: Geochemistry, Geophysics, Geosystems, v. 9, p. Q05Y01, doi: 10.1029/2007GC001856.

Kleinert, K., and Strecker, M.R., 2001, Climate change in response to orographic barrier uplift: Paleosol and stable isotope evidence from the late Neogene Santa Maria Basin, northwestern Argentina: Geological Society of America Bulletin, v. 113, no. 6, p. 728–742, doi: 10.1130/0016-7606(2001)113 <0728:CCIRTO>2.0.CO;2.

Kutzbach, J.E., Guetter, P.J., Ruddiman, W.F., and Prell, W.L., 1989, Sensitivity of climate to late Cenozoic uplift in southern Asia and the American West; numerical experiments: Journal of Geophysical Research, v. 94, no. D15, p. 18,393–18,407, doi: 10.1029/JD094iD15p18393.

Lease, R.O., Burbank, D.W., Gehrels, G.E., Wang, Z., and Yuan, D., 2007, Signatures of mountain building; detrital zircon U/Pb ages from northeastern Tibet: Geology (Boulder), v. 35, no. 3, p. 239–242, doi: 10.1130/G23057A.1.

Lee, J.-E., and Fung, I., 2008, "Amount effect" of water isotopes and quantitative analysis of post-condensation processes: Hydrological Processes, v. 22, p. 1–8, doi: 10.1002/hyp.6637.

Lee, J.-E., Fung, I., DePaolo, D.J., and Henning, C.C., 2007, Analysis of the global distribution of water isotopes using the NCAR atmospheric general circulation model: Journal of Geophysical Research, v. 112, p. D16, doi: 10.1029/2006JD007657.

Li, H.-C., and Ku, T.-L., 1997, $\delta^{13}C$-$\delta^{18}O$ covariance as a paleohydrological indicator for closed-basin lakes: Palaeogeography, Palaeoclimatology, Palaeoecology, v. 133, p. 69–80, doi: 10.1016/S0031-0182(96)00153-8.

Liu, B., Phillips, F.M., and Campbell, A.R., 1996, Stable carbon and oxygen isotopes of pedogenic carbonates, Ajo Mountains, southern Arizona: Implications for paleoenvironmental change: Palaeogeography, Palaeoclimatology, Palaeoecology, v. 124, p. 233–246, doi: 10.1016/0031-0182(95)00093-3.

Lourens, L.J., Hilgen, F.J., Laskar, J., Shackleton, N.J., and Wilson, D., 2005, The Neogene period, *in* Gradstein, F.M., Ogg, J.G., and Smith, A., eds., Geological Time Scale: Cambridge, UK, Cambridge University Press, p. 409–440.

Mack, G.H., James, W.C., and Monger, H.C., 1993, Classification of paleosols: Geological Society of America Bulletin, v. 105, no. 2, p. 129–136, doi: 10.1130/0016-7606(1993)105<0129:COP>2.3.CO;2.

McFadden, P.L., and McElhinny, M.W., 1990, Classification of the reversal test in paleomagnetism: Geophysical Journal International, v. 103, p. 725–729, doi: 10.1111/j.1365-246X.1990.tb05683.x.

McKenzie, J.A., Metcalf, R.L., and Stumm, W., 1985, Carbon isotopes and productivity in the lacustrine and marine environment: New York, John Wiley & Sons, p. 99–118.

Métivier, F., Gaudemer, Y., Tapponnier, P., and Meyer, B., 1998, Northeastward growth of the Tibet Plateau deduced from balanced reconstruction of two depositional areas; the Qaidam and Hexi Corridor basins, China: Tectonics, v. 17, no. 6, p. 823–842, doi: 10.1029/98TC02764.

Meyer, B., Tapponnier, T., Bourjot, L., Métivier, F., Gaudemer, Y., Peltzer, G., Guo, S., and Chen, Z., 1998, Crustal thickening in Gansu-Qinghai, lithospheric mantle subduction, and oblique, strike-slip controlled growth of the Tibet Plateau: Geophysical Journal International, v. 135, no. 1, p. 1–47, doi: 10.1046/j.1365-246X.1998.00567.x.

Mock, C., Arnaud, N.O., and Cantagrel, J.M., 1999, An early unroofing in northeastern Tibet? Constraints from $^{40}Ar/^{39}Ar$ thermochronology on granitoids from the eastern Kunlun range (Qianghai, NW China): Earth and Planetary Science Letters, v. 171, no. 1, p. 107–122, doi: 10.1016/S0012-821X(99)00133-8.

Molnar, P., 2004, Late Cenozoic increase in accumulation rates of terrestrial sediment: How might climate change have affected erosion rates?: Annual Review of Earth and Planetary Sciences, v. 32, p. 67–89, doi: 10.1146/annurev.earth.32.091003.143456.

Molnar, P., England, P., and Martinod, J., 1993, Mantle dynamics, uplift of the Tibetan Plateau, and the Indian monsoon: Reviews of Geophysics, v. 31, no. 4, p. 357–396, doi: 10.1029/93RG02030.

Poage, M.A., and Chamberlain, C.P., 2001, Empirical relationships between elevation and the stable isotope composition of precipitation and surface waters; considerations for studies of paleoelevation change: American Journal of Science, v. 301, no. 1, p. 1–15, doi: 10.2475/ajs.301.1.1.

Qinghai Bureau of Geology and Mineral Resources (QBGMR), 1991, Regional Geology of Qinghai Province: Beijing, Geological Publishing House, 662 p.

Quade, J., Garzione, C., Eiler, J., and Kohn, M.J., 2007, Paleoelevation reconstruction using pedogenic carbonates: Washington, D.C., Mineralogical Society of America and Geochemical Society, p. 53–87.

Raymo, M.E., and Ruddiman, W.F., 1992, Tectonic forcing of late Cenozoic climate: Nature, v. 359, no. 6391, p. 117–122, doi: 10.1038/359117a0.

Ritts, B.D., Yue, Y., Graham, S.A., Sobel, E.R., Abbink, O.A., and Stockli, D., 2008, From sea level to high elevation in 15 million years; uplift history of the northern Tibetan Plateau margin in the Altun Shan: American Journal of Science, v. 308, no. 5, p. 657–678, doi: 10.2475/05.2008.01.

Rozanski, K., Araguas-Araguas, L., and Gonfiantini, R., 1993, Isotopic patterns in modern global precipitation, *in* Swart, P.K., Lohman, K.C., McKenzie, J., and Savin, S., eds., Climate Change in Continental Isotopic Records: Washington, D.C., American Geophysical Union, Geophysical Monographs 78, p. 1–36.

Ruddiman, W.F., and Kutzbach, J.E., 1989, Forcing of late Cenozoic Northern Hemisphere climate by plateau uplift in southern Asia and the American West: Journal of Geophysical Research, v. 94, no. D15, p. 18,409–18,427, doi: 10.1029/JD094iD15p18409.

Savin, S.M., Douglas, R.G., and Stehli, F.G., 1975, Tertiary marine paleotemperatures: Geological Society of America Bulletin, v. 86, no. 11, p. 1499, doi: 10.1130/0016-7606(1975)86<1499:TMP>2.0.CO;2.

Scholl, M.A., Ingebritsen, S.E., Janik, C.J., and Kauahikaua, J.P., 1996, Use of precipitation and groundwater isotopes to interpret regional hydrology on a tropical volcanic island; Kilauea Volcano area, Hawaii: Water Resources Research, v. 32, no. 12, p. 3525–3537.

Takeuchi, A., and Larson, P.B., 2005, Oxygen isotope evidence for the late Cenozoic development of an orographic rain shadow in eastern Washington, USA: Geology, v. 33, no. 4, p. 313, doi: 10.1130/G21335.1.

Talbot, M.R., 1990, A review of the palaeohydrological interpretation of carbon and oxygen isotopic ratios in primary lacustrine carbonates: Chemical Geology, v. 80, p. 261–279.

Talbot, M.R., 1994, Paleohydrology of the late Miocene Ridge Basin lake, California: Geological Society of America Bulletin, v. 106, no. 9, p. 1121–1129, doi: 10.1130/0016-7606(1994)106<1121:POTLMR>2.3.CO;2.

Tapponnier, P., Xu, Z., Roger, F., Meyer, B., Arnaud, N., Wittlinger, G., and Yang, J., 2001, Oblique stepwise rise and growth of the Tibet Plateau: Science, v. 294, no. 5547, p. 1671–1677, doi: 10.1126/science.105978.

Tauxe, L., 1998, Paleomagnetic Principles and Practice: New York, Springer, 299 p.

Tauxe, L., and Gallet, Y., 1991, A jackknife for magnetostratigraphy: Geophysical Research Letters, v. 18, p. 1783–1786, doi: 10.1029/91GL01223.

Wang, E., Xu, F., Zhou, J., Wan, J., and Burchfiel, B.C., 2006, Eastward migration of the Qaidam basin and its implications for Cenozoic evolution of the Altyn Tagh fault and associated river systems: Geological Society of America Bulletin, v. 118, no. 3–4, p. 349–365, doi: 10.1130/B25778.1.

Wang, H., and Follmer, L.R., 1998, Proxy of monsoon seasonality in carbon isotopes from paleosols in the southern Chinese Loess Plateau: Geology, v. 26, no. 11, p. 987–990, doi: 10.1130/0091-7613(1998)026 <0987:POMSIC>2.3.CO;2.

Wang, Y., and Deng, T., 2005, A 25 m.y. isotopic record of paleodiet and environmental change from fossil mammals and paleosols from the NE margin of the Tibetan Plateau: Earth and Planetary Science Letters, v. 236, no. 1–2, p. 322–338, doi: 10.1016/j.epsl.2005.05.006.

Wang, Y., Deng, T., and Biasatti, D., 2006, Ancient diets indicate significant uplift of southern Tibet after ca. 7 Ma: Geology, v. 34, no. 4, p. 309–312, doi: 10.1130/G22254.1.

Yuan, D., Zhang, P., and Fang, X., 2007, Late Cenozoic tectonic deformation of the Linxia basin, northeastern margin of the Qinghai-Tibet Plateau: Earth Science Frontiers, v. 14, no. 1, p. 243–250 (in Chinese with English abstract).

Zachos, J., Pagani, M., Sloan, L., Thomas, E., and Billups, K., 2001, Trends, rhythms, and aberrations in global climate 65 Ma to present: Science, v. 292, no. 5517, p. 686, doi: 10.1126/science.1059412.

Zhai, Y., and Cai, T., 1984, The Tertiary system of Gansu province, *in* Gansu Geology: Lanzhou, China, Peoples Press of Gansu, p. 1–40.

Zheng, D., Zhang, P., Wan, J., Li, C., and Cao, J., 2003, Late Cenozoic deformation subsequence in northeastern margin of Tibet—Detrital AFT records from Linxia basin: Science in China, ser. D, Earth Science, v. 46, p. 266–275.

Zheng, D., Zhang, P.-Z., Wan, J., Yuan, D., Li, C., Yin, G., Zhang, G., Wang, Z., Min, W., and Chen, J., 2006, Rapid exhumation at ~8 Ma on the Liupan Shan thrust fault from apatite fission-track thermochronology: Implications for growth of the northeastern Tibetan Plateau margin: Earth and Planetary Science Letters, v. 248, no. 1–2, p. 198–208.

Zheng, D., Clark, M.K., Zhang, P., Zheng, W., and Farley, K.A., 2010, Erosion, fault initiation, and topographic growth of the North Qilian Shan (northern Tibetan Plateau): Geosphere (in press).

Manuscript Received 19 May 2009
Revised Manuscript Received 21 December 2009
Manuscript Accepted 21 May 2010

Printed in the USA